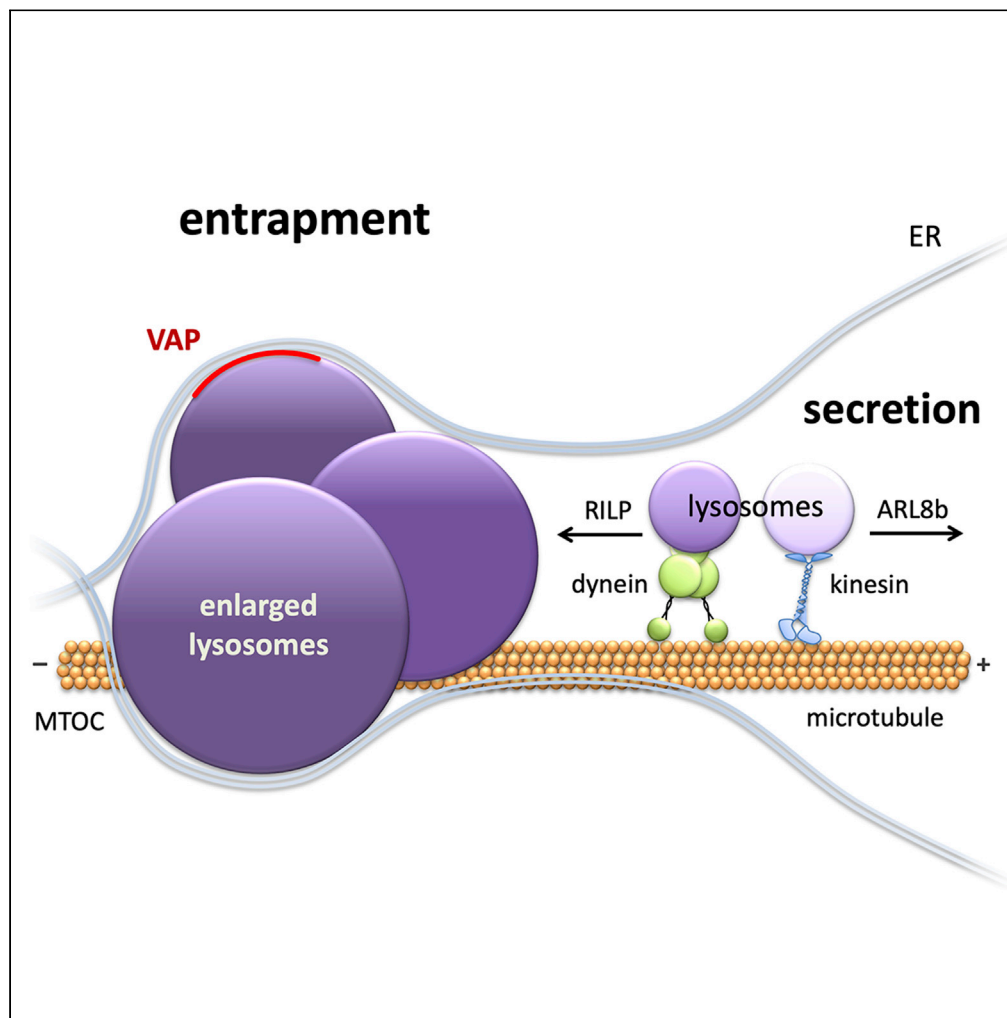


Article

Early onset effects of single substrate accumulation recapitulate major features of LSD in patient-derived lysosomes



Gianluca Scerra,  
Valeria De  
Pasquale, Luigi  
Michele Pavone,  
Maria Gabriella  
Caporaso,  
Andreas Mayer,  
Maurizio Renna,  
Massimo  
D'Agostino

andreas.mayer@unil.ch (A.M.)  
maurizio.renna@unina.it (M.R.)  
massimo.dagostino@unina.it  
(M.D.)

Highlights

LEU-ME triggers a rapid  
expansion of the  
lysosomal compartment

Expanded lysosomes  
display motility and  
secretion defects

Enlarged lysosomes  
display extended  
endoplasmic reticulum  
membrane contact sites

Scerra et al., iScience 24,  
102707  
July 23, 2021 © 2021 The  
Authors.  
[https://doi.org/10.1016/  
j.isci.2021.102707](https://doi.org/10.1016/j.isci.2021.102707)



## Article

## Early onset effects of single substrate accumulation recapitulate major features of LSD in patient-derived lysosomes

Gianluca Scerra,<sup>1</sup> Valeria De Pasquale,<sup>2</sup> Luigi Michele Pavone,<sup>1</sup> Maria Gabriella Caporaso,<sup>1</sup> Andreas Mayer,<sup>3,\*</sup> Maurizio Renna,<sup>1,\*</sup> and Massimo D'Agostino<sup>1,4,\*</sup>

## SUMMARY

**Lysosome functions mainly rely on their ability to either degrade substrates or release them into the extracellular space. Lysosomal storage disorders (LSDs) are commonly characterized by a chronic lysosomal accumulation of different substrates, thereby causing lysosomal dysfunctions and secretion defects. However, the early effects of substrate accumulation on lysosomal homeostasis have not been analyzed so far. Here, we describe how the acute accumulation of a single substrate determines a rapid centripetal redistribution of the lysosomes, triggering their expansion and reducing their secretion, by limiting the motility of these organelles toward the plasma membrane. Moreover, we provide evidence that such defects could be explained by a trapping mechanism exerted by the extensive contacts between the enlarged lysosomes and the highly intertwined membrane structures of the endoplasmic reticulum which might represent a crucial biological cue ultimately leading to the clinically relevant secondary defects observed in the LSD experimental models and patients.**

## INTRODUCTION

Lysosomes are organelles responsible for the degradation of a large variety of macromolecules derived from either inside or outside eukaryotic cells. Lysosomes accomplish such a fundamental function by fusing with cargo-containing organelles such as autophagosomes, Golgi-derived vesicles, as well as endosomes (Luzio et al., 2007; Schwake et al., 2013). In order to enable their degradative activity, lysosomes are equipped with different classes of acidic hydrolytic enzymes capable of digesting a variety of macromolecules, such as proteins, lipids, nucleic acids, and carbohydrates. In this regard, the activity of the vacuolar H<sup>+</sup>-ATPase pump plays a key role in generating and maintaining a highly acidic lumen, therefore providing the optimal environment for maximizing the activity of such hydrolytic enzymes (Mindell, 2012; Xiong and Zhu, 2016). Nonetheless, the function of the lysosomes is not confined to the mere degradation of macromolecules. Indeed, more recently the lysosomes have been identified as a key metabolic hub, influencing processes as diverse as nutrient sensing, secretion, gene regulation, plasma membrane repair, ions homeostasis, cholesterol transport, and immune response (Di Malta et al., 2012; Medina and Ballabio, 2015; Settembre and Ballabio, 2014).

Depending on its specific function, a single cell can host from tens to hundreds of lysosomes, which are highly heterogeneous in terms of pH (Johnson et al., 2016), subcellular localization (Willett et al., 2017), and morphology (Swanson et al., 1987). In addition, lysosomes can change and adapt their morphology depending on environmental cues, cellular specialization, growth conditions, and accumulation of substrates within their lumen.

Lysosomal storage disorders (LSDs) comprise about 70 rare genetic diseases characterized by a simple mendelian transmission, each specified by mutations in a single gene, which leads to the accumulation of specific substrates within the lysosomes, generally causing deleterious changes in morphology, as well as considerable defects in key lysosomal functions, including degradative activity, signaling, trafficking properties, and secretion (Kielian, 2019; Samie and Xu, 2014). In particular, the secretion defect has been associated with the progressive and chronic accumulation within the lysosomes of secondary substrates such as cholesterol, which impairs the membrane fusion machinery (Fraldi et al., 2010). Among LSDs,

<sup>1</sup>Department of Molecular Medicine and Medical Biotechnologies, University of Naples "Federico II", Naples, Italy

<sup>2</sup>Department of Veterinary Medicine and Animal Productions, University of Naples "Federico II", Naples, Italy

<sup>3</sup>Department of Biochemistry, University of Lausanne, Epalinges, Switzerland

<sup>4</sup>Lead contact

\*Correspondence: andreas.mayer@unil.ch (A.M.), maurizio.renna@unina.it (M.R.), massimo.dagostino@unina.it (M.D.)

<https://doi.org/10.1016/j.isci.2021.102707>



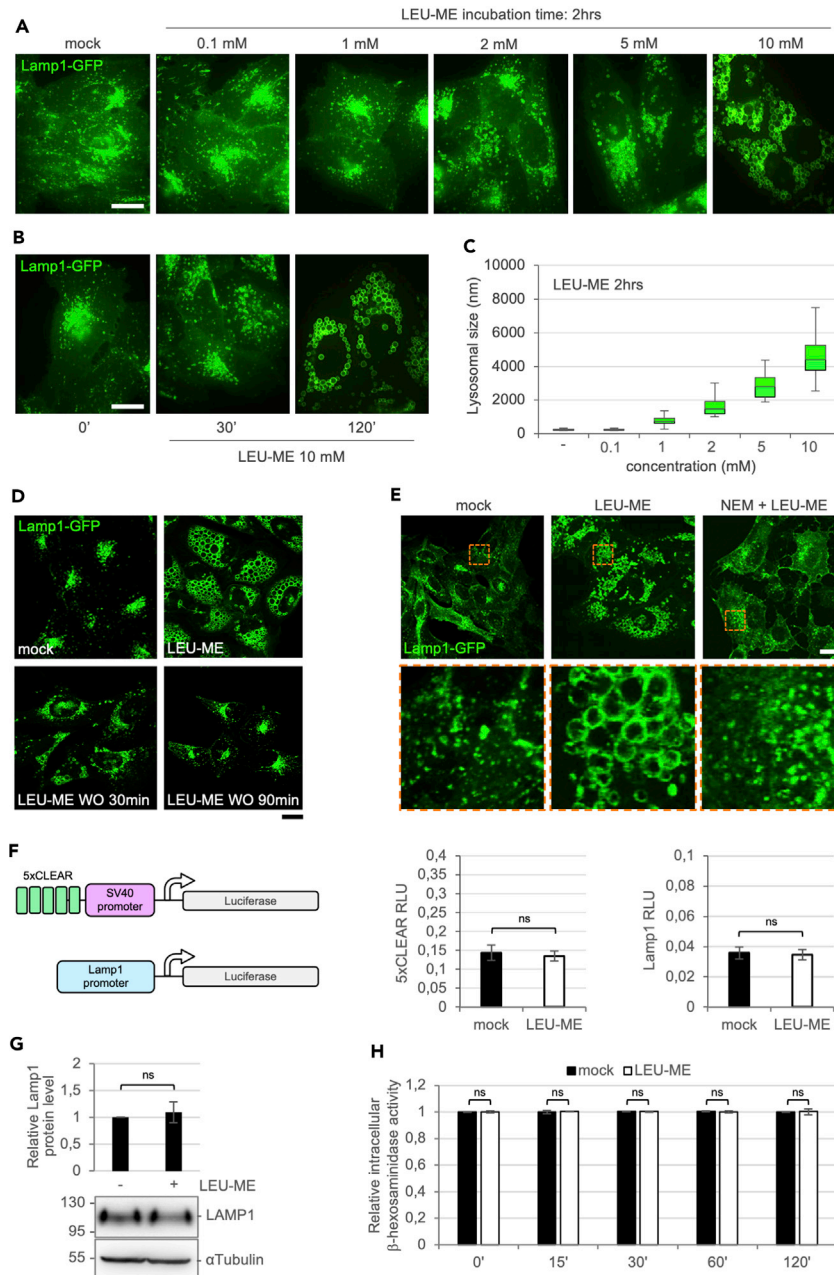


**Figure 1. Lysosomal morphology in LEU-ME treated cells**

(A and B) HeLa cells stably expressing the lysosomal marker Lamp1-GFP were treated with esterified leucine (LEU-ME) at increasing concentrations for 2 hr (A) or different time points (B), keeping constant the concentration of 10 mM.

(C) The histogram reports the quantification relative to the diameter of the Lamp1-GFP positive structures measured at different LEU-ME concentrations.

(D) Cells were treated as in a and the morphology of Lamp1-GFP positive structures was analyzed after 30 and 90 min of LEU-ME washout (WO).

(E) HeLa cells stably expressing the lysosomal marker Lamp1-GFP were pre-treated with 1 mM N-ethylmaleimide for 30 min before being exposed to LEU-ME 10 mM containing medium for 2 hr. Magnifications are shown in orange dashed squares. Scale bar: 50μm.

(F) HeLa cells were transiently transfected with the Luciferase vectors containing 5 TFEB-responsive elements (5xCLEAR) or Lamp1 promoter. The histogram reports the luciferase activity measured before and after 2 hr of treatment with LEU-ME.

**Figure 1. Continued**

(G) Total cell extracts of HeLa cells before and after treatment with LEU-ME 10mM for 2 hr, were separated by SDS-PAGE and Lamp1 protein level was analyzed by using a specific monoclonal antibody.  $\alpha$ Tubulin was used as loading control. (H) The histogram reports the relative intracellular  $\beta$ -hexosaminidase activity measured over time up to 120 min in presence or not of LEU-ME 10mM. Mean - values were obtained by three independent experiments. (ns) not statistically significant.

mucopolysaccharidoses (MPSs) are a group of diseases caused by the inherited deficiency of lysosomal enzymes involved in the degradation of glycosaminoglycans (GAGs) (Kakkis et al., 2001). The accumulation of undigested GAGs results in the loss of cellular functions, tissue damage, and organ dysfunction, ultimately leading to the most prominent MPS clinical manifestations, which include neurological disorders, as well as skeletal malformations, cardiac failure, hearing and vision impairment, and mental retardation (De Pasquale et al., 2020; De Pasquale and Pavone, 2019). Depending on the type of accumulated GAG, MPSs are classified into seven types (I, II, III, IV, VI, VII, and IX), which vary in terms of incidence and prevalence within the population, severity of clinical symptoms and morbidity (Muenzer, 2011). Despite the undeniable advancements in terms of therapeutic protocols designed to treat and alleviate the clinical symptoms of patients affected by MPS, a better understanding of the MPS physiopathology is still needed to develop even more effective therapeutic strategies to tackle these clinical conditions, whose prognosis is still largely unfavorable for most of the patients (De Pasquale et al., 2018a). In regard to the molecular pathogenesis of these diseases, the early effects of substrate accumulation on the homeostasis of the lysosomal compartment have not been thoroughly analyzed, so far. Hence, we report here how an early and short-term substrate accumulation within lysosomes phenocopies and recapitulates many of the long-term effects, such as lysosomes expansion, motility defects, and altered secretion, which are caused by its chronic accumulation. Our observations suggest that such defects are characterized by an early onset and are likely propaedeutic to the establishment of the severe lysosomal dysfunctions such as, among the others, an impaired lysosomal secretion, which represents a hallmark common to most of the LSDs. Finally, we provide an evidence-based working model according to which such a secretion defect could be consequent to a trapping mechanism caused by the tight association between the enlarged lysosomes and the dense membrane network of the endoplasmic reticulum (ER).

**RESULTS****Acute treatment with esterified amino acids causes a rapid expansion of the lysosomal compartment**

Chronic accumulation of undigested materials within the lysosomal lumen causes an expansion of the degradative compartment. Indeed, as shown in Figure S1A, the lysosomal compartment (i.e. Lamp1-positive structures) of human dermal fibroblasts derived from patients affected by Mucopolysaccharidosis-I and -IIIb (MPS-I and -IIIb) appeared remarkably expanded, when compared to human fibroblasts derived from healthy donors (HDFa). In addition, MPS-I and -IIIb fibroblast showed also a significantly impaired lysosomal secretion (Figure S1B). In order to study and experimentally assess the effect of an acute osmotic stress on lysosomal morphology and dynamics, HeLa cells stably expressing the endo-lysosomal protein marker Lamp1-GFP (Sbano et al., 2017) were treated with different amino acid analogs bearing a methyl-ester group (hereafter indicated as aa-ME). Such a chemical group makes them permeable to the biological membranes and, as such, able to reach various intracellular compartments. However, lysosomal hydrolases remove the methyl-ester group causing the accumulation of these amino acid analogs, ultimately generating an osmotic effect (Reeves, 1979). As shown in Figure S2, regardless of their physico-chemical properties, the short exposure (10 mM for 2 hr) to a number of methyl-ester modified amino acids, such as alanine (ALA-ME), leucine (LEU-ME) or histidine (HIS-ME) was able to trigger, although to a different extent, a considerable expansion of the lysosomal compartment (see the magnified panels in Figure S2). Such an effect was both concentration- and time-dependent (Figures 1A and B), leading to enlarged lysosomes, with an average diameter up to 5  $\mu$ m (Figure 1C).

As previously reported, the osmotic stress can lead to the rupture of the lysosomal membranes (Decker et al., 1985). However, LEU-ME treatment did not cause any evident signs of membrane rupture of the lysosomal compartment, as assessed by either live-cell imaging or by confocal microscopy performed on samples fixed with pure ice-cold methanol (Figure S3A, right and middle panels, respectively). Also, the imaging analysis performed with a well-known and commonly used permeable probe, such as LysoTracker, showed the usual and expected staining deriving from the lysosome lumen, therefore ruling out the

possibility of any alteration to the integrity of the lysosomal membranes induced by LEU-ME treatment (Figure S3B). Indeed, we could observe some features suggestive of lysosomal rupture exclusively following to formaldehyde-fixation (Figure S3A, left panels). Thus, we reasoned that an acute osmotic stress, such the one experimentally induced by LEU-ME, appears to make lysosomal membranes more sensitive to the fixation procedure, but without causing *per se* the rupture of lysosomal membranes *in vivo*. In fact, lysosomes might counterbalance an excessive tension operated on their membranes by increasing membrane fusion processes, in a similar way to the lysosome-like yeast vacuoles, a mechanism that we have previously described (D'Agostino et al., 2018; Desfougeres et al., 2016). Moreover, as shown in Figure 1D, within 90 min the lysosomes were able to regain their normal morphology, suggesting that the phenomenon is entirely reversible and that LEU-ME treatment does not hamper lysosomal fission processes. According to previous reports, upon removal of the aa analog, the enlarged lysosomes are expected to export the accumulated amino acid analogs from the lumen (Decker et al., 1985), thereby progressively dissipating the osmotic effect and re-activating the fission process. Indeed, we did confirm this was the case in HDFa cells (Figure S4), which mirrored the same behavior observed in HeLa cells (Figure 1D). We then went on to analyze the phenotype in LSDs patients-derived cells. Interestingly, in MPS-I and MPS-IIIb cells at steady-state, lysosomes already display a pathologically enlarged phenotype (Figure S4A). However, LEU-ME treatment was still able to induce a further expansion of the lysosomal compartment (Figure S4B). Perhaps even more importantly, such a phenomenon was reversible upon LEU-ME removal also in these cells (Figure S4C). Collectively, these results showed how both the fusion and fission machineries are still operative in the MPS cells and suggest that the enlarged size of the lysosomes is rather the consequence of a different fusion/fission equilibrium, reached by the progressive accumulation of undigested macromolecules within the lysosomal lumen.

Next, in order to determine whether this effect could result from the lysosomal swelling or rather from a membrane fusion process, cells were pre-treated with NEM (N-ethylmaleimide), which inhibits the AAA-ATPase NSF (N-ethylmaleimide sensitive factor) and therefore the SNARE-dependent membrane fusion (Malhotra et al., 1988). As shown in Figure 1E, NEM pre-treatment completely blocked the LEU-ME-dependent expansion of the lysosomes, suggesting that this expansion mainly relies on membrane fusion events. Moreover, such an expansion requires also the contribution, albeit partially, of the lysosomes-autophagosomes fusion, (Figure S5). In particular, by using HeLa cells stably expressing the RFP-GFP-LC3 reporter (Klionsky et al., 2012), we were able to simultaneously analyze both the size and the maturation of the autophagosomes under osmotic stress conditions (Figure S5A). As shown in Figures S5B and C, after 2 hr of exposure with LEU-ME, LC3-positive structures appeared considerably larger, compared to the mock-treated cells. The enlarged LC3-positive structures showed only RFP signal, indicating that autophagosome-lysosome fusion was still achieved, and that the acidic luminal pH was maintained. Furthermore, we showed how the observed expansion of the lysosomes was not functionally linked to an increase of the autophagosome biogenesis. Indeed, neither LC3B nor p62 protein level significantly changed in cells treated with LEU-ME alone or in combination with a saturating concentration of azithromycin, which blocks the autophagosomes turn-over (Figures S5D–F) (Renna et al., 2011) nor transcriptional activation of several key autophagic genes was observed (Figures S5G and H). Thus, we can conclude that 2 hr of lysosome overload with LEU-ME did not trigger an upregulation of the autophagic pathway. Consistent with this, we did not observe any significant transcriptional activation of the luciferase reporters under the control of the master regulator of lysosomes and autophagosomes biogenesis transcription factor EB (TFEB) (Sardiello et al., 2009; Settembre et al., 2011) or of the human Lamp1 promoter (Figure 1F). Overall, these data suggest how the lysosomes overload for 2 hr is not sufficient to trigger the activation of the TFEB-dependent transcriptional program. Finally, we analyzed within the same time frame the expression of the Lamp1 protein and the lysosomal enzyme  $\beta$ -hexosaminidase upon lysosomes overload. As shown in the Figure 1G, the expression of Lamp1 remained unchanged upon treatment with LEU-ME for 2 hr. On the same line, we did not observe any overt change in the activity of the intracellular  $\beta$ -hexosaminidase activity (used as proxy of its relative intracellular abundance) measured over time up to 2 hr of lysosomes overload (Figure 1H). Thus, these results indicate the expansion of the lysosomal compartment we do observe in the 2 hr time frame is the result of a membrane fusion-dependent process, rather than a lysosomal biogenesis-based mechanism.

### Osmotically enlarged lysosomes display secretion defect

Despite their major role being the degradation and/or recycling of cellular components, lysosomes are involved in other fundamental biological processes including, among the others, cellular secretion (Settembre et al., 2013). In order to test whether osmotically enlarged lysosomes were defective for secretion,

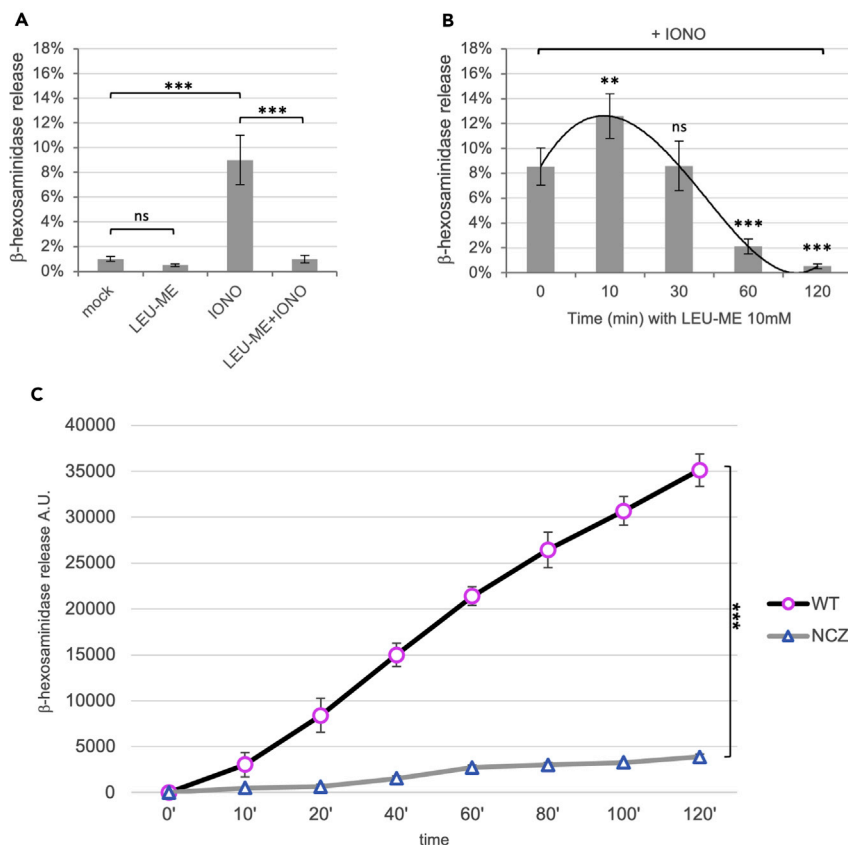


**Figure 2. Expanded lysosomes display secretion defect**

(A and B) The histograms report the percentage of  $\beta$ -hexosaminidase released from HeLa cells before and after stimulation with ionomycin (IONO) and before and after LEU-ME exposure at 10 mM for 2 hr (A) or over-time up to 120 min (B). The polynomial trend line is shown. c)  $\beta$ -hexosaminidase released from HeLa cells was measured over time up to 120 min in the absence or presence of the microtubule-depolymerizing agent nocodazole (NCZ). Mean - values were obtained by three independent experiments. Asterisks indicate the statistically significant differences: (\*\*\*) p value < 0.0001, (\*\*) p value < 0.001, (ns) not significant.

cells were treated with LEU-ME for 2 hr, and the release of a lysosomal resident enzyme, such as the  $\beta$ -hexosaminidase, was deployed as a readout for secretion, before and after a short exposure (i.e. 5 min) to the  $\text{Ca}^{2+}$  ionophore ionomycin, a widely used standard method to monitor the acute lysosomal secretion (Bennett et al., 1979; Sbrano et al., 2017). As shown in Figure 2A, in the absence of ionomycin (mock) only a small proportion (about 1%) of the  $\beta$ -hexosaminidase was found in the extracellular space, with this amount being further reduced after LEU-ME treatment (LEU-ME). As expected, upon induction with ionomycin (IONO), the secretion of the lysosomal enzyme increased up to 9–10%. The fraction of secreted enzyme was considerably reduced to only 2% upon ionomycin induction and in the presence of LEU-ME (LEU-ME + IONO), implying therefore that the detrimental effect operated by LEU-ME prevails over the one triggered by calcium. Moreover, since LEU-ME treatment provoked a progressive increase of lysosomal size (Figure 1C), we asked whether such an effect might proportionally affect lysosomal secretion, too. As shown in Figure 2B, the  $\beta$ -hexosaminidase secretion, triggered upon ionomycin exposure, progressively decreased down to the basal level, which can be observed in the absence of ionomycin induction. At 10 min, we recorded a significant increase of  $\beta$ -hexosaminidase secretion. Such an observation can be explained with the presence of a lysosomal subpopulation still capable of rapidly responding to ionomycin and inducing secretion, as opposed to a different subpopulation that remains confined within the cell.

Next, we analyzed constitutive lysosomes secretion (hence, in the absence of ionomycin treatment). As shown in Figure 2C,  $\beta$ -hexosaminidase was found to be constitutively secreted over time by the cells. Moreover, cells treated with nocodazole (NCZ), a potent depolymerizing agent of microtubules, displayed a

severe lysosome secretion defect, in comparison to the secretion measured in mock-treated cells. Taken together, these results suggest that the secretion defects could be strictly dependent on the lysosomal positioning within the cell.

### **Lysosomal positioning influences secretion defects caused by substrate accumulation**

Once expanded by LEU-ME treatment, the lysosomal compartment assumed a more perinuclear distribution, compared to what can be observed in mock-treated cells (Figures 3A and B), suggesting that under an acute osmotic stimulus, lysosomes moved toward the microtubule organizing center (MTOC), where the fusion with autophagosomes contributes to the final expansion of the degradative compartment. Thus, since the localization of the lysosomes is driven by motor and adaptor proteins such as dynein and RILP (favoring their perinuclear localization) (Cantalupo et al., 2001; Progida et al., 2007; Starling et al., 2016), or kinesins and ARL8b (which, conversely, drive lysosomes toward the cell periphery) (Bagshaw et al., 2006), we asked whether the overexpression of these GTPases could differently influence lysosomes secretion. As expected, RILP-GFP overexpression caused a massive re-localization of the lysosomes toward the MTOC (Cantalupo et al., 2001; Progida et al., 2007) (Figure 3C, upper panel). In this condition, lysosomes secretion was almost totally inhibited (Figure 3D), whereas ARL8b-HA overexpression, which redistributed the lysosomes to the cell periphery (Bagshaw et al., 2006) (Figure 3C, lower panel), resulted in a slightly but not significantly increase of basal secretion measured overtime for 2 hr (Figure 3D).

Furthermore, as shown in Figure S6A, the redistribution to the MTOC consequent to RILP-GFP overexpression caused a more pronounced expansion of the lysosomal compartment upon LEU-ME treatment when compared to the mock-transfected control cells, suggesting the evidence of a cumulative effect. Conversely, cells in which the lysosomes were peripherally redistributed by means of Arl8b-HA overexpression (Bagshaw et al., 2006) showed an almost complete lack of expansion of the compartment, in comparison to the mock-transfected cells (Figure S6B). All together, these data suggest that the re-localization to MTOC could represent one of the key steps that drives the expansion of the lysosomal compartment. As such, we asked whether a different distribution could differently affect lysosomes secretion upon substrate accumulation. To test this hypothesis, we overexpressed in HeLa cells ARL8b-HA, the full-length RILP-GFP and its cleaved form RILP-C33-GFP (Figure S7), which has been previously reported to affect the dynein-dependent lysosomes redistribution to the MTOC (Cantalupo et al., 2001) and to favor exosomes release (Willson, 2020). Cells were then treated with LEU-ME or iNPC1 (inhibitor of NPC1 that cause cholesterol accumulation within the lysosomes) (Lu et al., 2015) and either the induced (upon ionomycin stimulation) or constitutive lysosomal secretion were measured overtime for 2 hr by means of  $\beta$ -hexosaminidase release assay. As shown in Figure S8, iNPC1 treatment caused the expected cholesterol accumulation within the lysosomal lumen and, interestingly, a defect in the ionomycin-evoked secretion. Moreover, both LEU-ME or iNPC1 treatment, as well as RILP-GFP overexpression drastically reduced the constitutive secretion, whereas ARL8b-HA overexpression significantly improved  $\beta$ -hexosaminidase release (Figure 3E). Interestingly, RILP-C33-GFP overexpression did not significantly affect secretion. Nevertheless, it was able to counteract the inhibitory effect produced by LEU-ME or iNPC1 treatment and also to rescue the constitutive lysosome secretion. Taken together, these data suggest that, upon substrate accumulation, lysosomes moved toward the perinuclear area through an RILP-dynein complex-mediated mechanism. However, the expression of the truncated form of RILP is capable of redirect the lysosomal movement toward the cell periphery and to restore lysosomal secretion.

### **Enlarged lysosomes display motility defects**

In order to assess whether such a secretion defect could be due to an altered lysosome motility, HeLa cells stably expressing the lysosomal marker Lamp1-GFP were treated with LEU-ME for 2 hr and the movement of the lysosomes was tracked by time-lapse microscopy (Tsuruta et al., 2017). Consistent with a previously reported study aimed at analyzing the dynamic properties of late endosomes and lysosomes (Falcon-Perez et al., 2005), the behavior of Lamp1-GFP positive structures appeared as a combination of short- and long-range movement events in control cells (Figure 4A), with an average speed-track ranging from 0.3 to 1.3  $\mu\text{m/s}$  (Figure 4B). Upon LEU-ME treatment, Lamp1-GFP positive structures were found substantially stalled (Figures 4A and B).

In order to rule out the possibility that the observed phenomenon was restricted to the accumulation of amino acids within the lysosomes, HeLa cells were treated either with the iNPC or with chymostatin, a well-known inhibitor of lysosomal proteases, which produces similar defects on lysosomal morphology

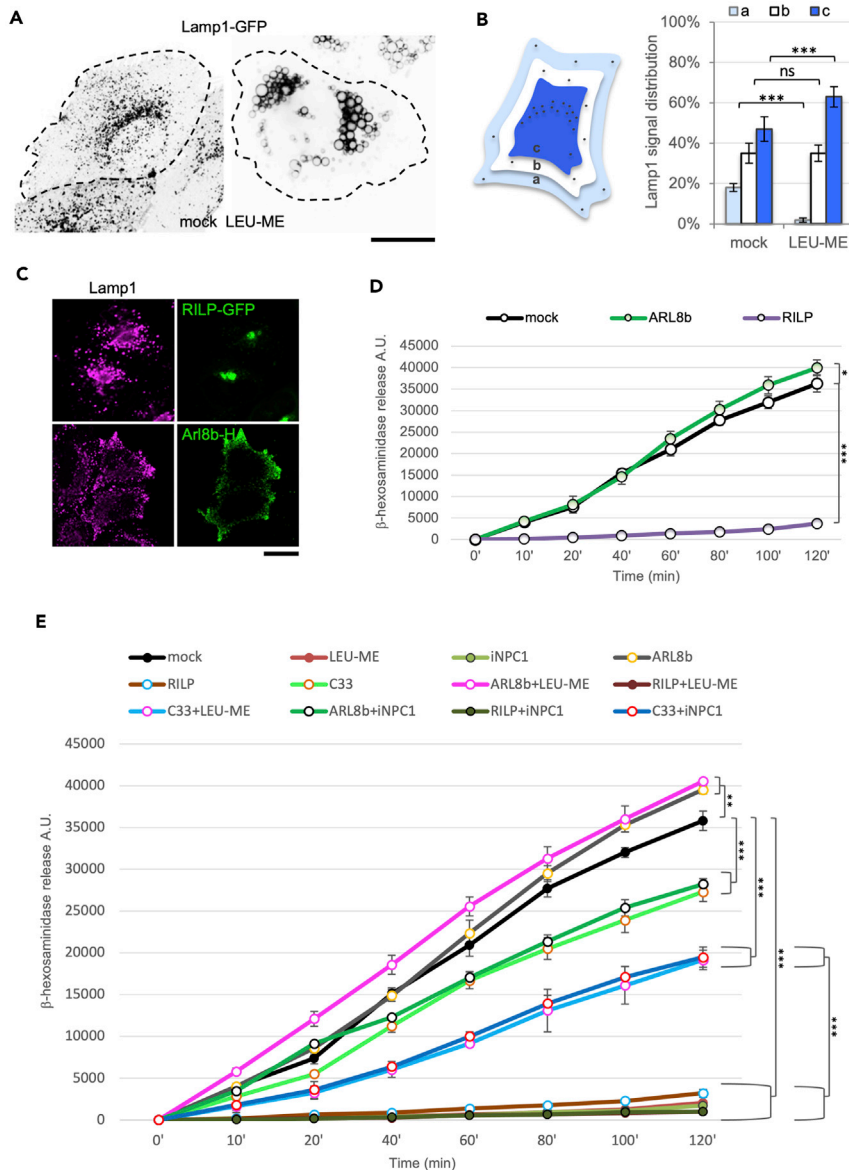


**Figure 3. Analysis of lysosomal distribution and constitutive secretion upon LEU-ME treatment**

(A and B) Lamp1-GFP positive structures positioning was analyzed before and after LEU-ME treatment (A) and its distribution within the cells is reported in the histogram (B).

(C) HeLa cells transiently transfected with RILP-GFP or Arl8b-HA (green signals) were analyzed by confocal microscopy by using a monoclonal antibody against the lysosomal protein marker Lamp1 (magenta signal). All images show single focal sections. Scale bar: 50  $\mu$ m.

(D) The histogram reports the constitutive  $\beta$ -hexosaminidase released over-time for 120 min from HeLa cells transiently transfected with RILP-GFP, Arl8b-HA.

(E) Constitutive  $\beta$ -hexosaminidase release assay was performed as in d in HeLa cells transiently transfected with the exogenous proteins and treated the indicated molecules (top legend). Mean - values were obtained by three independent experiments. Asterisks indicates the statistically significant differences: (\*\*\*) p value < 0.0001, (\*\*) p value < 0.001, (\*) p value < 0.05, (ns) not significant.

and secretion (Figure S9). Both treatments markedly decreased the motility of Lamp1-GFP positive structures (Figures 4C and D). Collectively, these data suggest that substrates of different nature, once accumulated within the lysosome, can exert similar detrimental effects on the motility and the trafficking properties of these organelles.

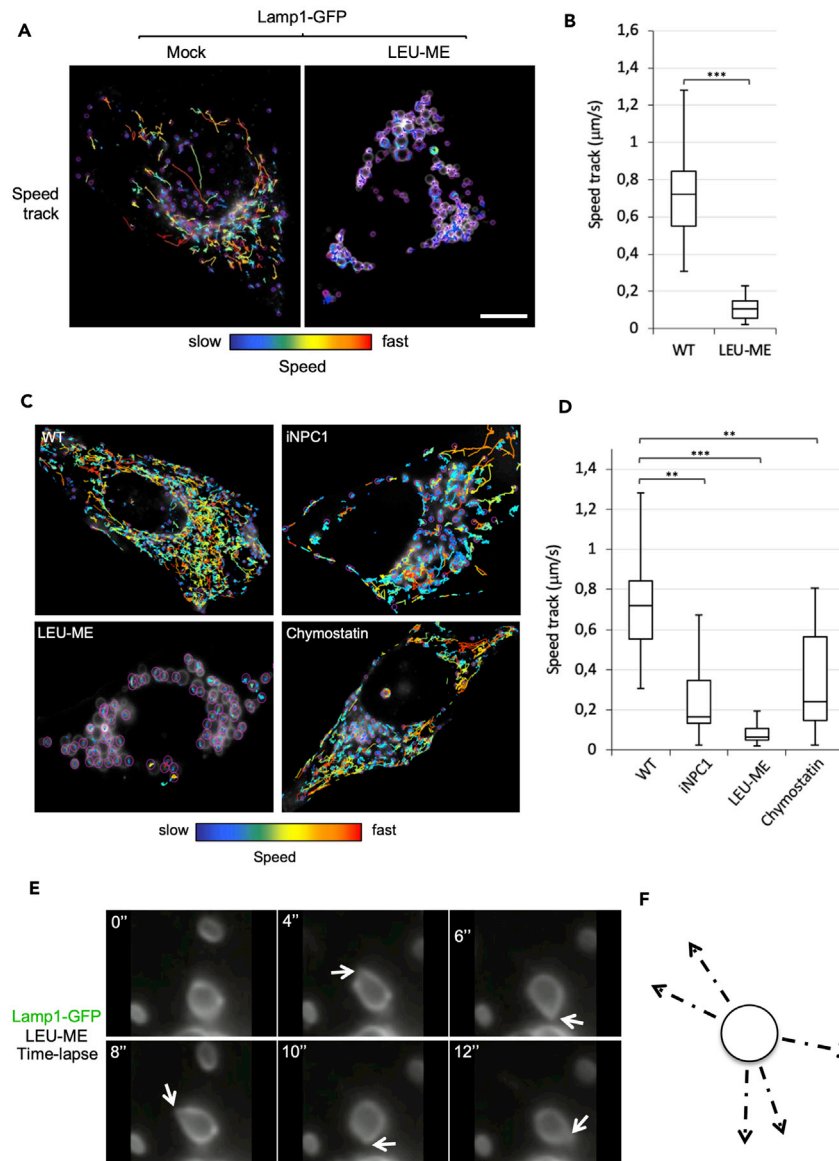


**Figure 4. Effect of LEU-ME treatment on lysosomal motility**

(A–D) Time-lapse microscopy was used to analyze Lamp1-GFP positive structures. Colors represent the kinetics of the movements of Lamp1-GFP positive structures (A and C) from slow (blue) up to fast (red). The histograms (B and D) report the quantifications relative to the speeds ( $\mu\text{m/s}$ ) of Lamp1-GFP positive structures analyzed in 30 cells for each experimental condition.

(E) Time-lapse microscopy was used to analyze the movement of a single Lamp1-GFP positive vesicle over time. White arrows indicate the appearance of membrane protrusions from the analyzed vesicle.

(F) Schematic view of the movement attempts of a single Lamp1-GFP positive vesicle. Single focal sections are shown. Mean - values were obtained by four independent experiments. Asterisks indicates the statistically significant differences: (\*\*\*)  $p$  value  $< 0.0001$ , (\*\*)  $p$  value  $< 0.001$ . Scale bar:  $50\mu\text{m}$ .

Since intracellular vesicular transport and directional movements are promoted by specialized motor proteins, the lack of mobility of the Lamp1-GFP positive structures could result from an alteration in the activity of these motor proteins or in their binding to the enlarged organelles, or both. Moreover, the perinuclear localization of these enlarged structures could limit their movement by generating a “traffic-jam” (i.e. by generating a steric hindrance effect). In view of these considerations, we analyzed by time-lapse microscopy the movements of the enlarged Lamp1-GFP-positive structures, primarily focusing on the pool of

vesicles outside the region of perinuclear clustering. When analyzed at higher magnification, the enlarged Lamp1-GFP-positive structures did not appear completely stalled, but they rather showed protrusions pointing into different directions at different timepoints. We reasoned that such a behavior could be likely expected if and/or when different (and differentially oriented) pulling forces, provided by individual motor proteins, act sequentially on different portions of a large vesicle that is locked-up in a defined place (Figures 4E and F). Thus, these results strongly suggest that enlarged Lamp1-GFP-positive structures could be simultaneously engaged and pulled by different motor proteins, ultimately causing a “tug-of-war” effect, which would ultimately explain the overall lack of (functional) mobility of these enlarged structures.

### Enlarged lysosomes affect ER and cytoskeleton organization by steric hindrance

We reasoned that lysosome expansion could lead to steric clashes and spatial competition with other organelles known to occupy most of the total volume of the cell, such as the ER or the cytoskeleton. In order to verify such a possibility, we first analyzed the morphology of the ER and microtubule organization in LEU-ME-treated cells. As shown in Figures 5A and C (lower panels), HeLa cells overexpressing mCherry-Sec61 $\beta$ , here used as ER marker, showed an altered ER organization, highlighted by the appearance of numerous black areas (i.e. areas not populated by ER membranes, indicated by white arrows in the magnified insets) upon LEU-ME treatment. Notably, these black areas appeared to be remarkably coincident and occupied by the enlarged Lamp1-GFP positive structures, illustrating an exclusion effect driven by steric hindrance. In addition, we did not find colocalization between these structures, as the ER membranes appeared to protrude and extend all around the enlarged lysosomes, thereby enwrapping them. Furthermore, the exclusion effect described above was particularly pronounced in regions of the cell occupied by clustered enlarged lysosomes (Figure 5A, yellow arrow), where ER membranes were almost completely absent. Similar alterations were observed when looking at the organization of the microtubules (Figures 5B and D). In particular, microtubules appeared to be pushed outward by the Lamp1-GFP enlarged structures upon LEU-ME treatment (as it can be better appreciated by looking at the structures indicated by white arrows in the magnified panels), confirming such a steric hindrance effect. Consistent with this, a very similar effect was also confirmed in cells treated with iNPC1, upon which lysosomes expansion caused similar alterations on both ER (Figures S10A and B) and cytoskeleton organization (Figures S10C and D).

### ER negatively influences the secretion of the enlarged lysosomes through a trapping mechanism

In view of the steric hindrance effect produced by the enlarged lysosomes on the ER membranes, we asked whether any variation of the ER density could, in turn, limit the motility and, as such, the secretion of enlarged lysosomes by trapping them. Thus, HeLa cells were treated with sodium palmitate (Palmitate), which is known to cause ER expansion (Kim et al., 2015) and the ER morphology was assessed by confocal imaging analysis of cells overexpressing the ER marker mCherry-Sec61 $\beta$ . As expected, upon treatment with Palmitate (400  $\mu$ M for 4 hr), cells displayed expanded ER cisternae (Figure 6A). Under these conditions, cells were treated with 10 mM LEU-ME, and  $\beta$ -hexosaminidase release was measured over time upon ionomycin induction. Strikingly, cells pre-treated with Palmitate showed an anticipated drop in secretion at 30–60 min, compared to the untreated cells, in which the drop in secretion was observed at 60–120 min (Figure 6B). This result suggests that the reduced secretion of enlarged lysosomes could be due to reduced motility, caused by their trapping into the ER membranes. Accordingly, a prolonged exposure to palmitate caused a significant (i.e. starting from 6 hr) reduction of lysosomal secretion (Figure S11). Consistent with the entrapment hypothesis, cells treated with a known microtubule-depolymerizing agent (nocodazole) caused the prompt lysosomal dispersion throughout the cytoplasm in control cells (Figures 6C and D, left panel and histogram, respectively), whereas enlarged lysosomes did not show such an effect (Figures 6C and D, right panel and histogram, respectively).

Finally, in view of the similarities, both in terms of morphology and distribution of the enlarged lysosomes, observed in HeLa and MPS cells upon LEU-ME treatment, we asked whether the ER and microtubule alterations could be observed also in MPS cells. As reported in Figure 7A, compared to the wild type HDFa cells, MPS-I and -IIIb cells displayed alterations of the ER and microtubular network very similar to the ones observed in the HeLa cells containing enlarged lysosomes. Moreover, the enlarged lysosomes of the MPS cells failed to diffuse through the cytosol and remained clustered upon treatment with nocodazole (Figure 7B, lower panels). By contrast, we were able to report the expected effect exerted by the nocodazole-induced microtubule disassembly in HDFa cells, which showed a significantly higher redistribution lysosomal dispersion (Figure 7B, left panels). All together, these data suggest how in two different cellular

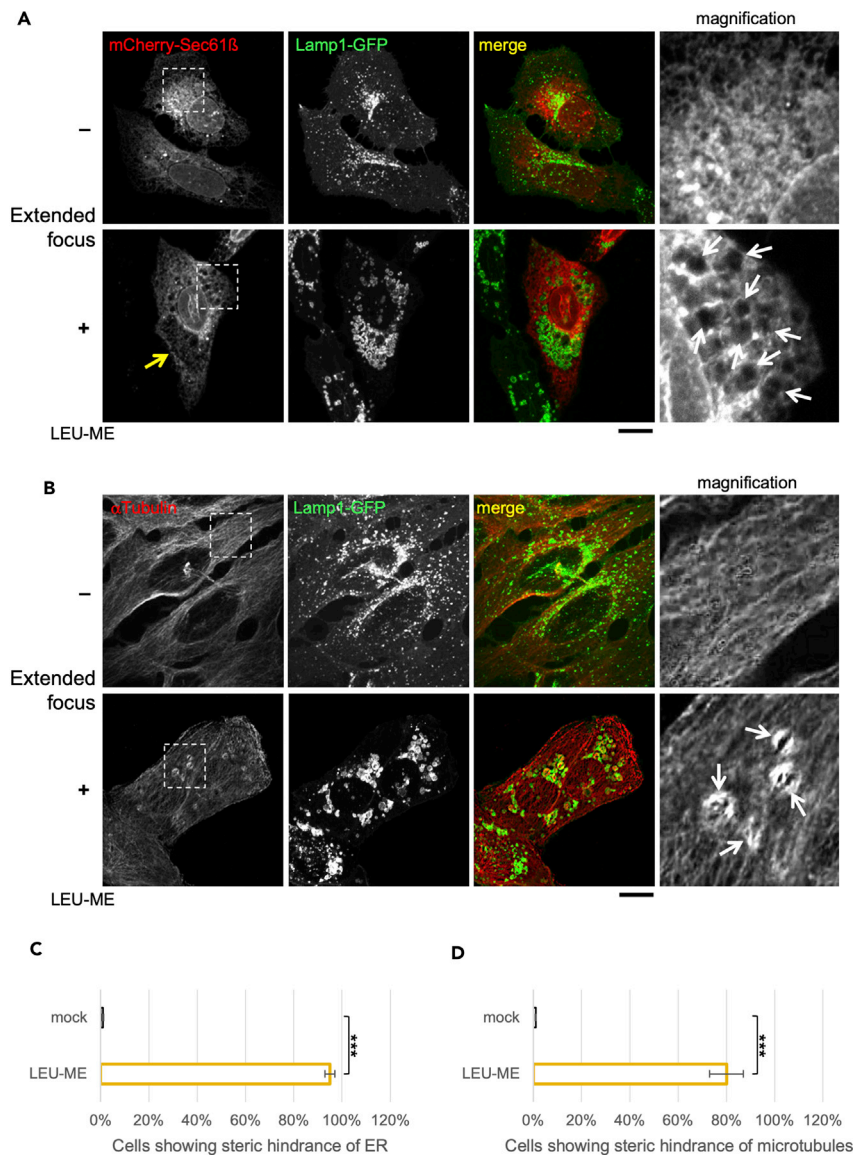


### Figure 5. ER morphology and microtubule organization upon LEU-ME treatment

(A and B) ER (revealed by overexpressing mCherry-Sec61β) and microtubule organization (revealed by using an antibody against αTubulin) were analyzed in HeLa cells stably expressing Lamp1-GFP before (-) and after (+) treatment with LEU-ME. Magnifications are shown in white dashed squares. White arrows indicate the exclusion area of the ER and the deformations zones of the microtubular network. Full projections are shown. Scale bar: 50μm.

(C and D) The histograms report the percentage of cells showing steric hindrance effect on ER (C) or microtubules (D). Mean - values were obtained by four independent experiments. Asterisks indicates the statistically significant differences: (\*\*\*) p value<0.0001.

models of lysosomal storage diseases (namely MPS-I and -IIIb), pathologically enlarged lysosomes could be retained within ER membranes, thereby ultimately limiting their motility and secretion.

### ER-lysosomal contact sites influence lysosomal morphology

It has been previously reported that ER proteins VAP (VAMP [vesicle-associated membrane protein]-associated ER protein) play a role in the definition of ER-lysosome membrane contact sites (MCSs) (Friedman et al., 2013; Rowland et al., 2014). Thus, we asked whether the enlarged lysosomes could affect the VAP-dependent ER-lysosomes MCSs. HeLa cells stably expressing Lamp1-GFP were transiently

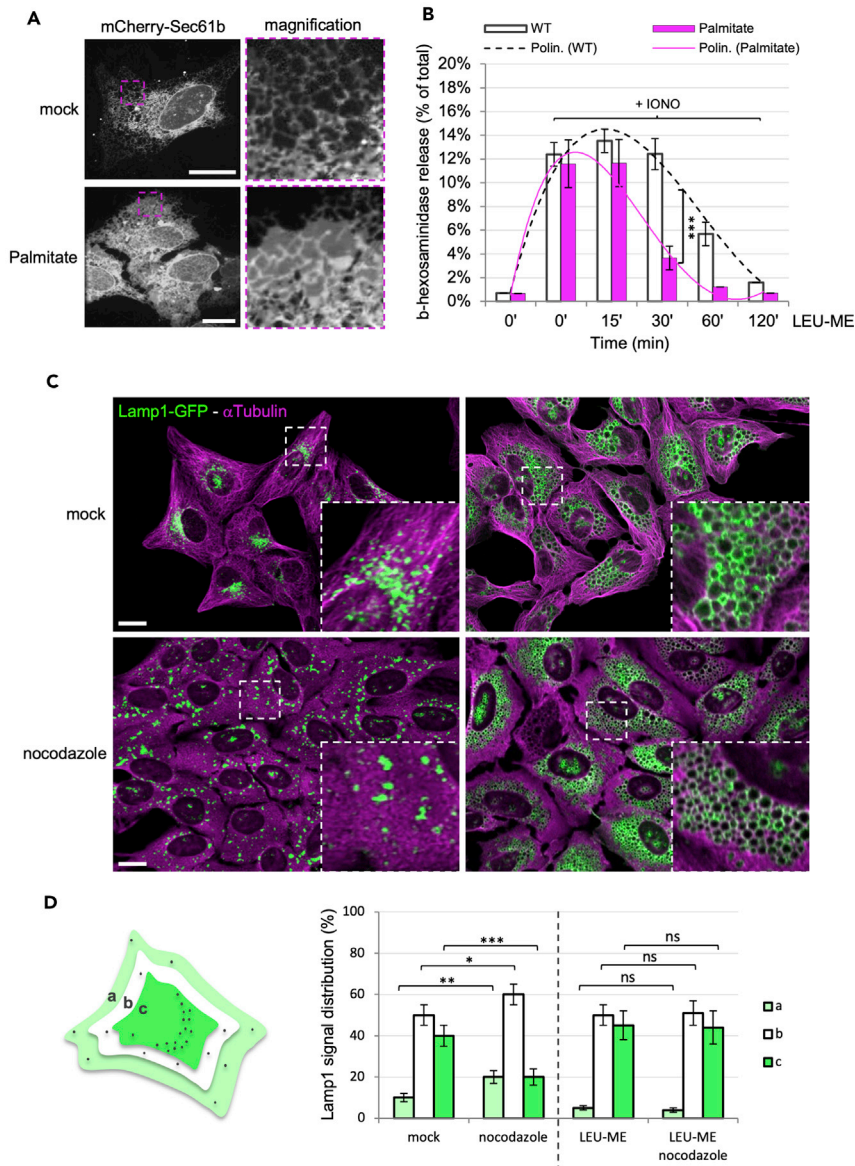


**Figure 6. Effect of the ER density on lysosomal secretion and distribution**

(A) The morphology of the ER (revealed by overexpressing mCherry-Sec61 $\beta$ ) was analyzed before and after treatment with sodium palmitate (400  $\mu$ M for 4 hr). Magnifications are shown in magenta dashed squares.

(B) The histogram reports the percentage of  $\beta$ -hexosaminidase released, triggered by ionomycin treatment (+IONO), analyzed in HeLa cells exposed to LEU-ME up to 120 min before (white bars) or after (magenta bars) pre-treatment with sodium palmitate. The polynomial trend lines are shown.

(C) Cells were pre-treated with LEU-ME or mock-treated, followed by treatment with 10  $\mu$ M nocodazole (microtubule-depolymerizing agent) for 2 hr. Lamp1-GFP positive structures were revealed before and after the nocodazole treatment. Microtubules organization was shown by using an antibody against  $\alpha$ -tubulin (magenta).

(D) The histogram reports the quantification of the relative distribution of Lamp1-GFP signals within the cells.

Magnifications are shown in white dashed squares. Single focal sections are shown. Mean values were obtained by three independent experiments. Asterisks indicate statistically significant differences: (\*\*\*) p value < 0.0001, (\*\*) p value < 0.001, (\*) p value < 0.05, (ns) not significant. Scale bar: 50  $\mu$ m.

transfected with VAPa-mCherry or VAPb-mCherry, and ER-lysosomes MCSs were analyzed by confocal microscopy. Upon LEU-ME treatment, VAP proteins were found particularly enriched over lysosomal membranes in a patched-like shape, suggesting extended ER-lysosomes MCSs (Figure 8A). Next, we asked

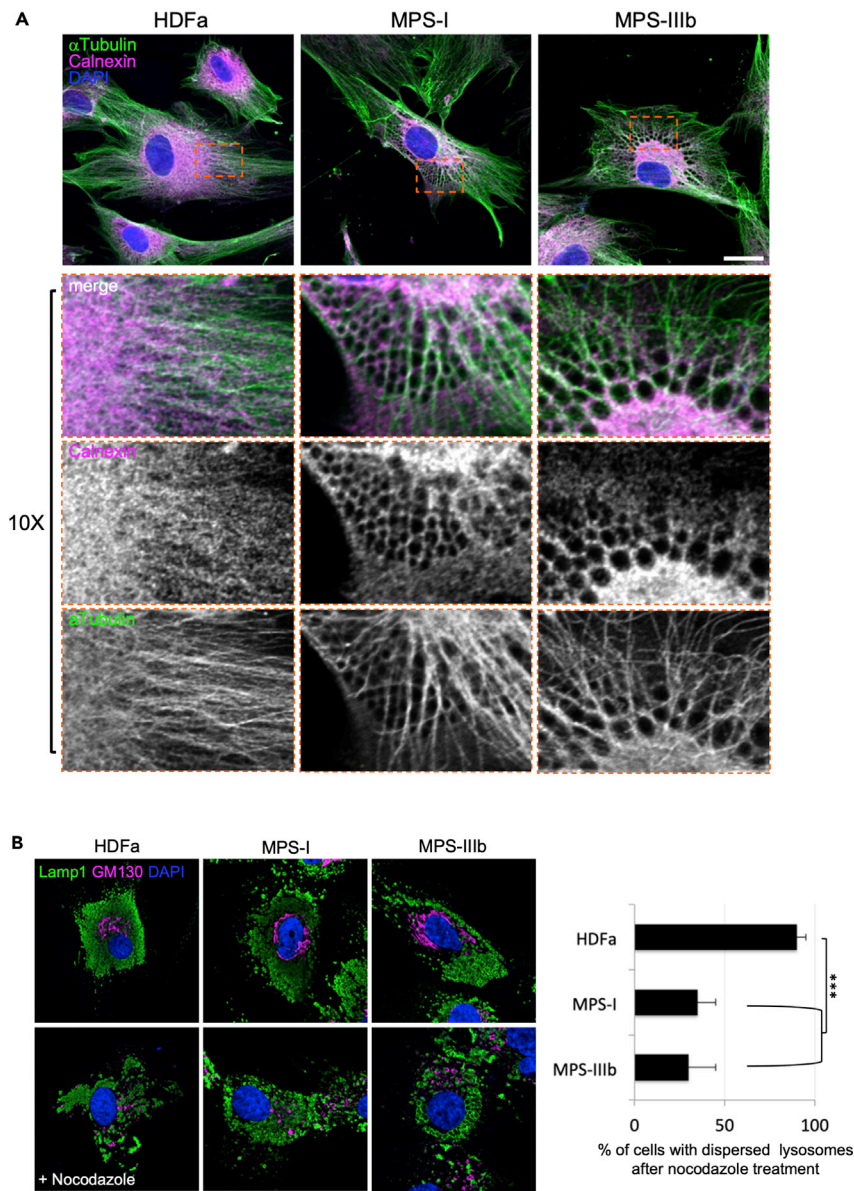


**Figure 7. ER morphology, microtubule organization and lysosome diffusion in MPS cells**

(A) Microtubule network organization and morphology of the ER in MPS cells were analyzed by using specific antibodies against  $\alpha$ Tubulin (microtubules, green) and Calnexin (ER marker, magenta). Nuclei were stained with DAPI. Magnifications are indicated in the orange dashed squares.

(B) MPS cells were grown as in a and treated with nocodazole 10  $\mu$ M for 2 hr before fixation. Lysosomes, Golgi and nuclei were revealed by using anti-Lamp1 (green signal), anti-GM130 (magenta signal) antibodies and DAPI (blue signal), respectively. The histogram reports the percentage of cells with dispersed lysosomes upon nocodazole treatment. Single focal sections are shown. Mean - values were obtained by four independent experiments. Asterisks indicates the statistically significant differences: (\*\*\*) p value < 0.0001. Scale bar: 50  $\mu$ m.

whether such a MCSs could have a functional role in lysosomes fission. In order to address this, we did perform VAP proteins depletion by RNA interference and looked at the ability of lysosomes to rescue their normal morphology in LEU-ME washout experiments. VAPa/b silencing did not affect the lysosomal expansion upon LEU-ME treatment (Figure 8B upper panels). However, after the washout (WO, lower panels) of LEU-ME, siCTRL cells rescued normal lysosomal morphology, whereas both siVAPa- or siVAPb-depleted cells failed to do so. This result suggests a possible role of VAP proteins in regulating lysosomal fission.

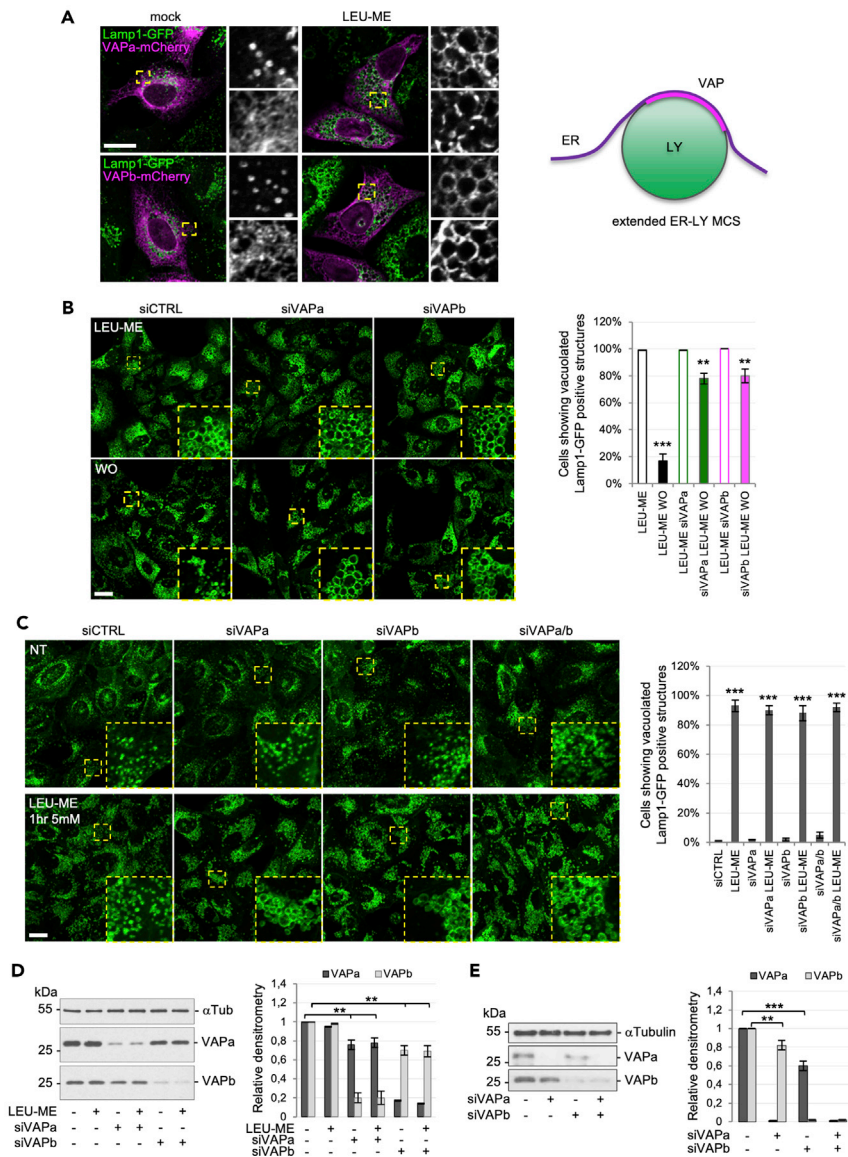


**Figure 8. Role of VAP proteins in lysosomes morphology**

(A) HeLa cells stably expressing Lamp1-GFP were transiently transfected with VAPa-mCherry or VAPb-mCherry and subcellular localization of chimeric VAP proteins was analyzed by confocal microscopy.

(B) Lysosome morphology was analyzed after LEU-ME treatment and its removal (WO) in mock or VAP silenced conditions. The histogram on the right shows the percentage of cells showing enlarged Lamp1-GFP positive structures.

(C) HeLa cells stably expressing Lamp1-GFP, singularly or in combination silenced or not for VAP proteins were treated with LEU-ME (5mM for 1hr) and lysosomes morphology was analyzed by confocal microscopy. The histogram on the right shows the percentage of cells showing enlarged Lamp1-GFP positive structures. Insets were shown in dashed yellow squares. Mean - values were obtained by three independent experiments.

(D) Western blotting and relative quantification (the histogram on the right) shows the extent of VAPs silencing before and after 5mM LEU-ME treatment for 1 hr.

(E) Western blotting and relative quantification (the histogram on the right) shows the impact VAPa silencing on VAPb protein expression and vice versa, and the extent of double VAPs silencing.

Asterisks indicates the statistically significant differences: (\*\*\*) p value<0.0001, (\*\*) p value<0.001, (\*) p value<0.05, (ns) not significant. Scale bar: 50μm.

Furthermore, since lysosomes can variate and adjust their size/number and morphology by constantly fine-tuning fusion and fission processes, we asked whether VAP proteins could have a role in regulating such a balance. In order to assess this, HeLa cells stably expressing Lamp1-GFP were silenced for either individual VAPs or in combination (siVAPa/b) and the morphology of lysosomes was analyzed upon a moderate LEU-ME treatment (i.e. both time wise – 1hr and concentration wise – 5mM, as detailed in the methods section), which determines a milder expansion effect on lysosomal compartment (as also reported in [Figures 1A–C](#)). As shown in [Figures 8C–E](#), the VAPs depletion did not cause *per se* any expansion effect compared to control cells, suggesting that under isotonic conditions fusion-fission processes still work to balance lysosomes morphology. Interestingly, upon treatment with suboptimal osmotic conditions (i.e. a lower LEU-ME concentration and for a shorter time), VAPs silenced cells showed larger lysosomes in comparison to the smaller size of Ctrl-treated cells. Taken together, these results confirm that VAPs have a role in ER-lysosomes MCSs and could participate in the fusion-fission balance process.

## DISCUSSION

In this study, we describe the early onset effects on the homeostasis of the lysosomal compartment that can be generated by the accumulation of a single substrate, such as an esterified amino acid analog. Such accumulation rapidly re-localizes lysosomes toward the MTOC, where their expansion is promoted by a membrane fusion process, which can increase the volume of the lysosomal compartment with the aim of counterbalancing the osmotic effect caused by the progressive accumulation of undigested substrates. This effect is in line with what has been described for the homotypic fusion of lysosome-like vacuoles in yeast ([Desfougeres et al., 2016](#)), where accumulation of materials caused the activation of SNARE proteins, a condition that favors fusion and the overall increase of the organelle volume. Increasing membrane tension may in addition counteract membrane fission, thereby shifting the membrane fusion/fission equilibrium further and ultimately causing the expansion of the vacuolar compartment. By these means, yeast can rapidly respond to the osmotic shocks, resizing the dimension of this fundamental compartment ([Desfougeres et al., 2016](#); [Michaillat et al., 2012](#); [Weisman, 2003](#)).

In our mammalian cell experimental system, steric hindrance by the ER and the cytoskeleton appears to cause a trapping effect, which strongly limits the motility of lysosomes toward the cell periphery. As a result, lysosomes secretion is strongly inhibited, which ultimately leads to a further accumulation of undigested substrates inside the cell. Lysosome redistribution toward the cell periphery, using Arl8b overexpression, interferes with the expansion of the compartment and prevents the lysosomes secretion defect. By contrast, lysosome re-localization toward the MTOC favors the lysosomal expansion, exacerbating the secretion defect. Lysosomal positioning could therefore play a key role in controlling and fine-tuning the size of the organelle and the dynamic balance between two functionally distinct lysosomal subpopulations, namely a “secretion-prone” and a “secretion-restricted” pool. Accordingly, the increase in the releasable pool of lysosomes through substrate accumulation likely suggests that lysosome secretion might be one way by which cells might seek to avoid accumulation of lysosomal storage products, providing an interesting physiological perspective to the observations described in our work. Such a secretion could be “internally” triggered by the lysosome itself because lysosomes contain TRP channels, which are mechano-sensitive and can be opened by membrane tension ([Liedtke and Kim, 2005](#)). In such a scenario, it is conceivable to speculate that the overloaded lysosome itself might release the calcium necessary for its fusion. If this occurs at the cell periphery, it will prompt secretion. Conversely, by occurring in lysosome localized toward the perinuclear area, it might rather trigger Ca<sup>2+</sup>-dependent homotypic membrane fusion, ultimately increasing lysosome volume. Consistent with this, under the overload condition, the interference with centripetal localization of the lysosomes by overexpressing a truncated form of RILP (RILP-C33) ([Figure 3E](#)) triggers lysosome secretion. Most importantly, we did not observe such a phenomenon in the absence of LEU-ME overload, suggesting that the lysosome’s movement toward the center or the periphery of the cell depends on the motor machinery recruited in response to the substrate accumulation. Such an observation is also in agreement with a previously proposed model, according to which the Rab7-to-Arl8b switch controls the late-endosomal transport ([Jongsma et al., 2020](#)). Thus, the Rab7-RILP-dynein motor complex might be preferentially recruited once substrates start to accumulate within lysosomes and the activation/recruitment of such a complex could be controlled by signals raised in response to a mechanical stimulus, such as the increased membrane tension induced by the substrates accumulating within the lumen of lysosomes.

Enlarged lysosomes become visibly entrapped at the cell center. This phenomenon is well illustrated by the membrane protrusions that arise from the enlarged lysosomes, which are nonetheless neither able to move the entire organelle nor to operate the membrane tubulation and vesicles excision ([Figure 4E](#)). Moreover,

both in HeLa cells treated with esterified amino acid analogs or in primary fibroblasts derived from MPS-I and MPS-IIIb patients, enlarged lysosomes failed to re-localize within the cytoplasm, upon microtubule disassembly (Figures 6 and 7). The entrapment of the enlarged lysosomes will hinder them from reaching the plasma membrane and in this way contribute to the lysosomal secretion defect observed in several LSDs, as well as in other different hereditary pathologies (Brandt et al., 1975; Park et al., 2016; Samie and Xu, 2014). In addition, the endo-lysosomal compartments are able to modulate their activities as a function of their positioning in the cell (Cabukusta and Neefjes, 2018; Wandinger-Ness and Zerial, 2014).

At the moment, the study of MCSs represents one of the most pioneering fields of investigation in cell biology. ER-endosome, ER-late endosome (LE), and ER-lysosome MCSs have been shown to be highly dynamic and common within mammalian cells (Eden et al., 2010). Interestingly, it has been shown how ER-LE MCSs appeared to define sites of vesicle scission at the LE, from which small tubules sprouted and vesicles budded, implying an active role for the ER in endosomal dynamics and also potentially suggesting that the ER may contribute to provide the mechanical force to the vesicle for the scission reaction (Friedman et al., 2013; Rowland et al., 2014). In our work, we provide evidence that enlarged lysosomes establish extended ER-lysosomes MCSs where ER-anchor membrane VAP proteins are found enriched (Figure 8A). Moreover, we found that, upon release of the osmotic condition causing the enlarged phenotype (LEU-ME washout experiments), lysosomes fail to rescue normal morphology when VAP proteins are down-modulated, likely suggesting a possible role played by these proteins regulating an ER-lysosomes MCSs-dependent membrane fission system. Thus, we think that VAP proteins might cooperate in the lysosomal fission process; as such, it is possible to envisage how upon an osmotic condition, lysosomes do enlarge and the pressure-generated, intraluminal outward force outweighs the mechanical force exerted on the membranes, impairing their deformation, prolonging the time for binding and ultimately contributing to the lack of mobility of these organelles. Moreover, VAPs silencing did not suppress the osmotic-dependent lysosomes expansion thereby ruling out a direct involvement in such process. Still, these results allowed us to temporally and spatially dissect the role of VAPs in lysosomes expansion. We think that, under osmotic stress, lysosomes re-localize in an RILP/dynein-dependent manner to the MTOC, where they fuse causing the steric hindrance on ER and cytoskeleton structures. These extended and prolonged contacts are responsible of two key defects: (i) lysosomes movement become disordered and unproductive, likely because the insurgence of extended and/or atypical contacts with microtubules could promote the engagement of multiple divergent motor proteins; (ii) in consideration of the role of VAP proteins in lysosome membrane fission, the ER membranes could establish extended MCSs with enlarged lysosomes in the attempt to re-establish their normal morphology but failing because of the higher membrane tension osmotically produced as a consequence of the intra-luminal accumulation of substrates.

Many factors can influence the morphology of intracellular organelles (Chan and Marshall, 2010; Hara and Kimura, 2011; Marshall, 2012). One of these is the size of a compartment as a function of the volume of the entire cell, which appears to be fairly well preserved among different cell types. Such phenomenon is defined as *organelle-cell size scaling* (Chan and Marshall, 2010). However, new types of questions arise when one considers organelles together rather than individually. As an example, organelles must be packed together in a confined volume. Thus, one could ask whether the expansion of one individual organelle leads to (or rather requires) the compression of others. This is still an open question, and it needs to be addressed in order to understand how a cell is built and maintained (Marshall, 2020). Our results do provide yet another example of how the size of an organelle must be tightly controlled and re-adjusted with respect to the size/volume of other organelles, in order to avoid any imbalance that could hamper its activity and functionality. In this regard, it appears reasonable to envisage that the size of a lysosome must be limited in order to allow it to move through the extensive ER and microtubular networks in the cytosol, avoiding it to become entangled and arrested. Several examples of selective organelle expansion or contraction occur during cell differentiation and tissue morphogenesis and may be related to such requirements. For instance, the differentiation of B lymphocytes into plasma cells does require a remarkable reorganization and expansion of the ER and of the secretory pathway, which is instrumental to the massive production of immunoglobulins (Kirk et al., 2010). On the same line, other cells of the immune system, such as granulocytes, despite not being able of a comparable biosynthetic activity, do possess large lysosome-like granules, which they are able to promptly secrete in order to exert their cell-killing activity (Bainton, 1999; Sheshachalam et al., 2014). In view of our experimental observations, we could speculate that a massive biosynthetic activity concomitant to the secretion of lysosome-like organelles could be perhaps incompatible at a cellular level. The co-existence of an expanded and dense ER for massive production of antibodies would most likely generate physical constraints that would impede granule motility and secretion. From this

perspective, it may not come as a coincidence that immature granulocytes display an extended ER, which they substantially reduce upon maturation. The ER then also assumes a peculiar morphology characterized by wide canaliculi or vesicles, which is very different from the typical branched ER structure (Anderson, 1966; Sorenson, 1960). This more open and disperse structure may result more functional to the movement and secretion of the large secretory vesicles in the mature granulocyte. Thus, we propose that expansion and structure of different cellular compartments may have to be adjusted in a coordinated manner in order to guarantee their functional interplay. Overall, such a process could be defined as “*organelle-to-organelle size scaling*”. The experimental observations described in our work suggest that an imbalance of organelle-organelle size scaling can contribute to the insurgence of pathological conditions, such as the LSDs.

### Limitation of study

In this work, we analyzed the effects of an acute accumulation of a single artificial substrate within lysosomes. In pathological situations, the initial accumulation of a single substrate is less acute and more progressive. This could lead to the activation of the lysosomal responses at a different time window and the onset of lysosomal dysfunctions at a different degree.

### STAR★METHODS

Detailed methods are provided in the online version of this paper and include the following:

- **KEY RESOURCES TABLE**
  - Cell culture
  - Plasmids, cell transfections, and silencing
  - Immunoblotting
  - Fluorescence microscopy
  - Lysosome distribution and dispersion measurement
  - Ionomycin treatment and  $\beta$ -hexosaminidase release assay
  - RNA isolation and real-time PCR
  - Luciferase reporter assays
  - Quantification of the steric hindrance
- **QUANTIFICATION AND STATISTICAL ANALYSIS**

### SUPPLEMENTAL INFORMATION

Supplemental information can be found online at <https://doi.org/10.1016/j.isci.2021.102707>.

### ACKNOWLEDGMENTS

This work was partially funded by a Telethon Grant GGP14002 to S.B., ERC Grant 233458 to A.M., and Italian Minister for Research and University (PRIN 20177XJCHX) to M.R., and departmental funding to M.D.A. We would like to thank professors David Rubinsztein (Cambridge Institute for Medical Research, UK), Maria Antonietta De Matteis (Tigem, Pozzuoli, IT), and Stefano Bonatti (DMMBM, UNINA, IT) for sharing reagents, scientific support, and helpful discussions. The Cell Line and DNA Biobank from patients affected by genetic diseases (Istituto G. Gaslini), member of the Telethon Network of Genetic Biobanks (project GTB12001), funded by Telethon Italy, provided us with specimens (fibroblasts from MPS patients).

### AUTHOR CONTRIBUTIONS

This work was conceived by M.D.A. and A.M. with the contribution of M.R. The experiments were designed and performed by M.D.A., G.S., and V.D.P. L.M.P. provided MPS cells. The manuscript was written by M.D.A., A.M., M.R. and L.M.P. All the authors read, revised and edited the manuscript.

### DECLARATION OF INTERESTS

The authors declare no competing financial interests.

Received: November 23, 2020

Revised: April 6, 2021

Accepted: June 8, 2021

Published: July 23, 2021

REFERENCES

- Anderson, D.R. (1966). Ultrastructure of normal and leukemic leukocytes in human peripheral blood. *J. Ultrastruct. Res.* 9, 1–42.
- Bagshaw, R.D., Callahan, J.W., and Mahuran, D.J. (2006). The Arf-family protein, Arl8b, is involved in the spatial distribution of lysosomes. *Biochem. Biophys. Res. Commun.* 344, 1186–1191.
- Bainton, D.F. (1999). Distinct granule populations in human neutrophils and lysosomal organelles identified by immuno-electron microscopy. *J. Immunol. Methods* 232, 153–168.
- Bennett, J.P., Cockcroft, S., and Gomperts, B.D. (1979). Ionomycin stimulates mast cell histamine secretion by forming a lipid-soluble calcium complex. *Nature* 282, 851–853.
- Brandt, E.J., Elliott, R.W., and Swank, R.T. (1975). Defective lysosomal enzyme secretion in kidneys of Chediak-Higashi (beige) mice. *J. Cell Biol.* 67, 774–788.
- Cabukusta, B., and Neefjes, J. (2018). Mechanisms of lysosomal positioning and movement. *Traffic* 19, 761–769.
- Caiazza, C., D’Agostino, M., Passaro, F., Faicchia, D., Mallardo, M., Paladino, S., Pierantoni, G.M., and Tramontano, D. (2019). Effects of long-term citrate treatment in the PC3 prostate cancer cell line. *Int. J. Mol. Sci.* 20, 2613.
- Cantalupo, G., Alifano, P., Roberti, V., Bruni, C.B., and Bucci, C. (2001). Rab-interacting lysosomal protein (RILP): the Rab7 effector required for transport to lysosomes. *EMBO J.* 20, 683–693.
- Cerulo, G., Tafuri, S., De Pasquale, V., Rea, S., Romano, S., Costagliola, A., Della Morte, R., Avallone, L., and Pavone, L.M. (2014). Serotonin activates cell survival and apoptotic death responses in cultured epithelial thyroid cells. *Biochimie* 105, 211–215.
- Chan, Y.H., and Marshall, W.F. (2010). Scaling properties of cell and organelle size. *Organogenesis* 6, 88–96.
- Ciano, M., Allocca, S., Ciardulli, M.C., Della Volpe, L., Bonatti, S., and D’Agostino, M. (2016). Differential phosphorylation-based regulation of alphaB-crystallin chaperone activity for multipass transmembrane proteins. *Biochem. Biophys. Res. Commun.* 479, 325–330.
- D’Agostino, M., Crespi, A., Polishchuk, E., Generoso, S., Martire, G., Colombo, S.F., and Bonatti, S. (2014). ER reorganization is remarkably induced in COS-7 cells accumulating transmembrane protein receptors not competent for export from the endoplasmic reticulum. *J. Membr. Biol.* 247, 1149–1159.
- D’Agostino, M., Risselada, H.J., Endter, L.J., Comte-Miserez, V., and Mayer, A. (2018). SNARE-mediated membrane fusion arrests at pore expansion to regulate the volume of an organelle. *EMBO J.* 37, e99193.
- D’Agostino, M., Scerra, G., Cannata Serio, M., Caporaso, M.G., Bonatti, S., and Renna, M. (2019). Unconventional secretion of alpha-Crystallin B requires the Autophagic pathway and is controlled by phosphorylation of its serine 59 residue. *Sci. Rep.* 9, 16892.
- De Pasquale, V., Moles, A., and Pavone, L.M. (2020). Cathepsins in the pathophysiology of mucopolysaccharidoses: new perspectives for therapy. *Cells* 9, 979.
- De Pasquale, V., and Pavone, L.M. (2019). Heparan sulfate proteoglycans: the sweet side of development turns sour in mucopolysaccharidoses. *Biochim. Biophys. Acta Mol. Basis Dis.* 1865, 165539.
- De Pasquale, V., Pezone, A., Sarogni, P., Tramontano, A., Schiattarella, G.G., Avvedimento, V.E., Paladino, S., and Pavone, L.M. (2018a). EGFR activation triggers cellular hypertrophy and lysosomal disease in NAGLU-depleted cardiomyoblasts, mimicking the hallmarks of mucopolysaccharidosis IIIB. *Cell Death Dis.* 9, 40.
- De Pasquale, V., Sarogni, P., Pistorio, V., Cerulo, G., Paladino, S., and Pavone, L.M. (2018b). Targeting heparan sulfate proteoglycans as a novel therapeutic strategy for mucopolysaccharidoses. *Mol. Ther. Methods Clin. Dev.* 10, 8–16.
- Decker, R.S., Decker, M.L., and Thomas, V. (1985). Protein degradation and lysosomal proteinases in cultured fetal rabbit cardiac myocytes. *Prog. Clin. Biol. Res.* 180, 627–628.
- Desfougères, Y., Neumann, H., and Mayer, A. (2016). Organelle size control - increasing vacuole content activates SNAREs to augment organelle volume through homotypic fusion. *J. Cell Sci.* 129, 2817–2828.
- Di Malta, C., Fryer, J.D., Settembre, C., and Ballabio, A. (2012). Autophagy in astrocytes: a novel culprit in lysosomal storage disorders. *Autophagy* 8, 1871–1872.
- Eden, E.R., White, I.J., Tsapara, A., and Futter, C.E. (2010). Membrane contacts between endosomes and ER provide sites for PTP1B-epidermal growth factor receptor interaction. *Nat. Cell Biol.* 12, 267–272.
- Falcon-Perez, J.M., Nazarian, R., Sabatti, C., and Dell’Angelica, E.C. (2005). Distribution and dynamics of Lamp1-containing endocytic organelles in fibroblasts deficient in BLOC-3. *J. Cell Sci.* 118, 5243–5255.
- Filocamo, M., Baldo, C., Goldwurm, S., Renieri, A., Angelini, C., Moggio, M., Mora, M., Merla, G., Politano, L., Garavaglia, B., et al. (2013). Telethon Network of Genetic Biobanks: a key service for diagnosis and research on rare diseases. *Orphanet J. Rare Dis.* 8, 129.
- Fraldi, A., Annunziata, F., Lombardi, A., Kaiser, H.J., Medina, D.L., Spampinato, C., Fedele, A.O., Polishchuk, R., Sorrentino, N.C., Simons, K., et al. (2010). Lysosomal fusion and SNARE function are impaired by cholesterol accumulation in lysosomal storage disorders. *EMBO J.* 29, 3607–3620.
- Friedman, J.R., Dibenedetto, J.R., West, M., Rowland, A.A., and Voeltz, G.K. (2013). Endoplasmic reticulum-endosome contact increases as endosomes traffic and mature. *Mol. Biol. Cell* 24, 1030–1040.
- Hara, Y., and Kimura, A. (2011). Cell-size-dependent control of organelle sizes during development. *Results Probl. Cell Differ.* 53, 93–108.
- Johnson, D.E., Ostrowski, P., Jaumouille, V., and Grinstein, S. (2016). The position of lysosomes within the cell determines their luminal pH. *J. Cell Biol.* 212, 677–692.
- Jongsma, M.L., Bakker, J., Cabukusta, B., Liv, N., van Elstrand, D., Fermie, J., Akkermans, J.L., Kuijl, C., van der Zanden, S.Y., Janssen, L., et al. (2020). SKIP-HOPS recruits TBC1D15 for a Rab7-to-Arl8b identity switch to control late endosome transport. *EMBO J.* 39, e102301.
- Kakkis, E.D., Muenzer, J., Tiller, G.E., Waber, L., Belmont, J., Passage, M., Izykowski, B., Phillips, J., Doroshov, R., Walot, I., et al. (2001). Enzyme-replacement therapy in mucopolysaccharidosis I. *N. Engl. J. Med.* 344, 182–188.
- Kielian, T. (2019). Lysosomal storage disorders: pathology within the lysosome and beyond. *J. Neurochem.* 148, 568–572.
- Kim, S.K., Oh, E., Yun, M., Lee, S.B., and Chae, G.T. (2015). Palmitate induces cisternal ER expansion via the activation of XBP-1/CC1alpha-mediated phospholipid accumulation in RAW 264.7 cells. *Lipids Health Dis.* 14, 73.
- Kirk, S.J., Cliff, J.M., Thomas, J.A., and Ward, T.H. (2010). Biogenesis of secretory organelles during B cell differentiation. *J. Leukoc. Biol.* 87, 245–255.
- Klionsky, D.J., Abdalla, F.C., Abeliovich, H., Abraham, R.T., Acevedo-Arozena, A., Adeli, K., Agholme, L., Agnello, M., Agostini, P., Aguirre-Ghiso, J.A., et al. (2012). Guidelines for the use and interpretation of assays for monitoring autophagy. *Autophagy* 8, 445–544.
- Kusama, Y., Sato, K., Kimura, N., Mitamura, J., Ohdaira, H., and Yoshida, K. (2009). Comprehensive analysis of expression pattern and promoter regulation of human autophagy-related genes. *Apoptosis* 14, 1165–1175.
- Liedtke, W., and Kim, C. (2005). Functionality of the TRPV subfamily of TRP ion channels: add mechano-TRP and osmo-TRP to the lexicon! *Cell Mol. Life Sci.* 62, 2985–3001.
- Livak, K.J., and Schmittgen, T.D. (2001). Analysis of relative gene expression data using real-time quantitative PCR and the 2<sup>-</sup>(Delta Delta C(T)) Method. *Methods* 25, 402–408.
- Lu, F., Liang, Q., Abi-Mosleh, L., Das, A., De Brabander, J.K., Goldstein, J.L., and Brown, M.S. (2015). Identification of NPC1 as the target of U18666A, an inhibitor of lysosomal cholesterol export and Ebola infection. *Elife* 4, e12177.
- Luzio, J.P., Pryor, P.R., and Bright, N.A. (2007). Lysosomes: fusion and function. *Nat. Rev. Mol. Cell Biol.* 8, 622–632.
- Malhotra, V., Orci, L., Glick, B.S., Block, M.R., and Rothman, J.E. (1988). Role of an N-ethylmaleimide-sensitive transport component in promoting fusion of transport vesicles with cisternae of the Golgi stack. *Cell* 54, 221–227.

- Marshall, W.F. (2012). Organelle size control systems: from cell geometry to organelle-directed medicine. *Bioessays* 34, 721–724.
- Marshall, W.F. (2020). Scaling of subcellular structures. *Annu. Rev. Cell Dev. Biol.* 36, 219–236.
- Medina, D.L., and Ballabio, A. (2015). Lysosomal calcium regulates autophagy. *Autophagy* 11, 970–971.
- Michaillat, L., Baars, T.L., and Mayer, A. (2012). Cell-free reconstitution of vacuole membrane fragmentation reveals regulation of vacuole size and number by TORC1. *Mol. Biol. Cell* 23, 881–895.
- Mindell, J.A. (2012). Lysosomal acidification mechanisms. *Annu. Rev. Physiol.* 74, 69–86.
- Muenzer, J. (2011). Overview of the mucopolysaccharidoses. *Rheumatology (Oxford)* 50 (Suppl 5), v4–v12.
- Park, S., Ahuja, M., Kim, M.S., Brailoiu, G.C., Jha, A., Zeng, M., Baydyuk, M., Wu, L.G., Wassif, C.A., Porter, F.D., et al. (2016). Fusion of lysosomes with secretory organelles leads to uncontrolled exocytosis in the lysosomal storage disease mucopolipidosis type IV. *EMBO Rep.* 17, 266–278.
- Progida, C., Malerod, L., Stuffers, S., Brech, A., Bucci, C., and Stenmark, H. (2007). RILP is required for the proper morphology and function of late endosomes. *J. Cell Sci.* 120, 3729–3737.
- Reeves, J.P. (1979). Accumulation of amino acids by lysosomes incubated with amino acid methyl esters. *J. Biol. Chem.* 254, 8914–8921.
- Renna, M., Schaffner, C., Brown, K., Shang, S., Tamayo, M.H., Hegyi, K., Grimsey, N.J., Cusens, D., Coulter, S., Cooper, J., et al. (2011). Azithromycin blocks autophagy and may predispose cystic fibrosis patients to mycobacterial infection. *J. Clin. Invest.* 121, 3554–3563.
- Rowland, A.A., Chitwood, P.J., Phillips, M.J., and Voeltz, G.K. (2014). ER contact sites define the position and timing of endosome fission. *Cell* 159, 1027–1041.
- Samie, M.A., and Xu, H. (2014). Lysosomal exocytosis and lipid storage disorders. *J. Lipid Res.* 55, 995–1009.
- Sardiello, M., Palmieri, M., di Ronza, A., Medina, D.L., Valenza, M., Gennarino, V.A., Di Malta, C., Donaudo, F., Embrione, V., Polishchuk, R.S., et al. (2009). A gene network regulating lysosomal biogenesis and function. *Science* 325, 473–477.
- Sbano, L., Bonora, M., Marchi, S., Baldassari, F., Medina, D.L., Ballabio, A., Giorgi, C., and Pinton, P. (2017). TFEB-mediated increase in peripheral lysosomes regulates store-operated calcium entry. *Sci. Rep.* 7, 40797.
- Schwake, M., Schroder, B., and Saftig, P. (2013). Lysosomal membrane proteins and their central role in physiology. *Traffic* 14, 739–748.
- Settembre, C., and Ballabio, A. (2014). Lysosomal adaptation: how the lysosome responds to external cues. *Cold Spring Harb. Perspect. Biol.* 6, a016907.
- Settembre, C., Di Malta, C., Polito, V.A., Garcia Arencibia, M., Vetrini, F., Erdin, S., Erdin, S.U., Huynh, T., Medina, D., Colella, P., et al. (2011). TFEB links autophagy to lysosomal biogenesis. *Science* 332, 1429–1433.
- Settembre, C., Fraldi, A., Medina, D.L., and Ballabio, A. (2013). Signals from the lysosome: a control centre for cellular clearance and energy metabolism. *Nat. Rev. Mol. Cell Biol.* 14, 283–296.
- Sheshachalam, A., Srivastava, N., Mitchell, T., Lacy, P., and Eitzen, G. (2014). Granule protein processing and regulated secretion in neutrophils. *Front. Immunol.* 5, 448.
- Sorenson, G.D. (1960). An electron microscopic study of hematopoiesis in the liver of the fetal rabbit. *Am. J. Anat.* 106, 27–40.
- Starling, G.P., Yip, Y.Y., Sanger, A., Morton, P.E., Eden, E.R., and Dodding, M.P. (2016). Folliculin directs the formation of a Rab34-RILP complex to control the nutrient-dependent dynamic distribution of lysosomes. *EMBO Rep.* 17, 823–841.
- Swanson, J., Burke, E., and Silverstein, S.C. (1987). Tubular lysosomes accompany stimulated pinocytosis in macrophages. *J. Cell Biol.* 104, 1217–1222.
- Tsuruta, F., Okajima, T., Yano, S., and Chiba, T. (2017). Quantification of endosome and lysosome motilities in cultured neurons using fluorescent probes. *J. Vis. Exp.* 123, 55488.
- Wandinger-Ness, A., and Zerial, M. (2014). Rab proteins and the compartmentalization of the endosomal system. *Cold Spring Harb. Perspect. Biol.* 6, a022616.
- Weisman, L.S. (2003). Yeast vacuole inheritance and dynamics. *Annu. Rev. Genet.* 37, 435–460.
- Willett, R., Martina, J.A., Zewe, J.P., Wills, R., Hammond, G.R.V., and Puertollano, R. (2017). TFEB regulates lysosomal positioning by modulating TMEM55B expression and JIP4 recruitment to lysosomes. *Nat. Commun.* 8, 1580.
- Willson, J. (2020). RILP gets cleaved and exosomes leave. *Nat. Rev. Mol. Cell Biol.* 21, 658–659.
- Xiong, J., and Zhu, M.X. (2016). Regulation of lysosomal ion homeostasis by channels and transporters. *Sci. China Life Sci.* 59, 777–791.

STAR★METHODS

KEY RESOURCES TABLE

REAGENT or RESOURCE	SOURCE	IDENTIFIER
<b>Antibodies</b>		
mouse monoclonal anti-CD107a (anti-Lamp1)	Sigma-Aldrich	#SAB4700416; RRID:AB_10932380
rabbit polyclonal anti-Calnexin	Stress Marq Biosciences	#SPC-108; RRID: AB_2069000
rabbit polyclonal anti VAPa and VAPb	Kindly provided by prof. Maria Antonietta De Matteis (Venditti R. et al. 2019)	N/A
rabbit polyclonal anti-LC3B	Novus Biologicals	NB100-2220; RRID:AB_10003146
mouse monoclonal anti-SQSTM1 D-3 (p62)	Santa Cruz Biotechnology	sc-28359; RRID:AB_628279
mouse and rabbit Alexa-Fluor (488 and 546) secondary antibodies	Thermo Fisher Scientific-Invitrogen	A11029; RRID:AB_138404, A11030; RRID:AB_144695, A11034; RRID:AB_2576217, A11035; RRID:AB_143051
mouse monoclonal (HRP)-conjugated secondary antibody	Amersham Pharmacia	GTxMu-003-DHRPX; RRID:AB_2884989
rabbit monoclonal (HRP)-conjugated secondary antibody	Amersham Pharmacia	GTxRb-003-DHRPX; RRID:AB_2884989
<b>Plasmids</b>		
GFP-RILP	Kindly provided by prof. Cecilia Buccì (Cantalupo G. et al. 2001)	N/A
GFP-RILP-C33	Kindly provided by prof. Cecilia Buccì (Cantalupo G. et al. 2001)	N/A
pCI-neo-Arl8b-HA	GenScript	N/A
mCherry-Sec61b	ADDGENE	#90994; RRID:Addgene_90994
VAPa-mCherry	Kindly provided by prof. Maria Antonietta De Matteis (Venditti R. et al. 2019)	N/A
VAPb-mCherry	Kindly provided by prof. Maria Antonietta De Matteis (Venditti R. et al. 2019)	N/A
pGL3-LC3 promoter-Luciferase	Kindly provided by prof. Yoshida K. (Kusama et al., 2009).	N/A
pGL3-Atg16L1 promoter-Luciferase	Kindly provided by prof. Yoshida K. (Kusama et al., 2009).	N/A
pGL3-Atg4B promoter-Luciferase	Kindly provided by prof. Yoshida K. (Kusama et al., 2009).	N/A
pGL3-ULK1 promoter-Luciferase	Kindly provided by prof. Yoshida K. (Kusama et al., 2009).	N/A
pGL3-CONTROL-Luciferase	Promega	U47296; RRID:Addgene_69915
Lamp1 promoter-Luciferase	RenSP Active Motif	#32001; RRID:Addgene_32001
<b>Cell lines</b>		
Primary Human Dermal Fibroblast from MPSI and IIIb patients	Cell Line and DNA Biobank from Patients Affected by Genetic Diseases (Filocamo et al., 2013)	N/A
Primary Human Dermal Fibroblast	Gibco	C0135C; RRID:CVCL_K404
HeLa cells stably expressing RFP-GFP-LC3	Kindly provided by prof. David C. Rubinsztein	N/A
HeLa cells stably expressing Lamp1-mGFP	Kindly provided by prof. Andrea Ballabio	N/A

(Continued on next page)

**Continued**

REAGENT or RESOURCE	SOURCE	IDENTIFIER
<b>Chemicals</b>		
Dulbecco Modified Eagle's Medium	Microgem	AL007A
Bovine serum albumin	Filipek	#107
Fetal Calf Serum	Microgem	S1810-500
Oxoid™ Phosphate Buffered Saline Tablets	Thermo Fisher Scientific-Invitrogen	BR0014G
ECL System	Bio-Rad	170-5061
Bio-Rad Protein Assay Dye Reagent concentrate	Bio-Rad	#5000006
Nocodazole	Sigma-Aldrich	#M1404
Sodium Palmitate	Sigma-Aldrich	#P9767
Chymostatin	Sigma-Aldrich	#C7268
Protease inhibitor cocktail tablets	Roche Diagnostics	4693116001
Filipin	Sigma-Aldrich	#F9765
Formaldehyde solution 37%	Sigma-Aldrich	#F15587
Methanol	Sigma-Aldrich	#34860
Trizma base	Sigma-Aldrich	#1503
Glycine	Sigma-Aldrich	#G8898
Acrylamide/Bis-acrylamide, 30% solution	Sigma-Aldrich	#A3699
Ionomycin calcium salt from Streptomyces conglobatus	Sigma-Aldrich	#I0634
4-methyl-umbelliferyl-N-acetyl-β-D-glucosaminide	Sigma-Aldrich	#M2133
U18666A, inhibitor of NPC1	Sigma-Aldrich	#662015
L-Leucine methyl-ester hydrochloride	Sigma-Aldrich	#L1002
L-Alanine methyl-ester hydrochloride	Sigma-Aldrich	#330639
L-Histidine methyl-ester dihydrochloride	Sigma-Aldrich	#H15403
ProLong™ Gold Antifade Mountant with DAPI	Thermo Fisher Scientific-Invitrogen	#P36935
SensiFAST SYBR Lo-ROX 2x Mix	Meridian	BIO-94020
TRIsure	Bioline	BIO-38033
Ionomycin calcium salt from Streptomyces conglobatus	Sigma-Aldrich	#I0634
<b>Critical commercial assays</b>		
High-Capacity RNA-to-cDNA Kit	Applied Biosystems	REF 4387406
MicroAmp Fast Optical 96-Well Reaction Plate	Applied Biosystems	REF 4346906
QuantStudio 7 Flex instrument	Thermo Fisher Scientific-Invitrogen	4485701
Dual-Glo Luciferase assay kit	Promega	E2920
<b>Oligonucleotides for Real-time PCR</b>		
LC3A Fw: 5'-GTGAGTGTGCCACGCCCAT-3' Rv: 5'-AGGTTTCCTGGGAGCGTAG-3'	Invitrogen	N/A
GAPDH Fw: 5'-GTCGGAGTCAACGGATTTGG-3' Rv: 5'-AAAAGCAGCCCTGGTGACC-3'	Invitrogen	N/A
<b>Software and algorithms</b>		
QuantStudio 6 and 7 Flex	Applied Biosystems	N/A
Fiji ImageJ	National Institutes of Health	N/A

### Cell culture

HeLa cells were grown at 37°C in Dulbecco's modified essential medium (DMEM), containing 10% fetal bovine serum (FBS), 100 U/ml Penicillin/Streptomycin, 2 mM L-Glutamine (L-Gln). HeLa cells stably expressing Lamp1-mGFP were grown in the same medium, supplemented with 400 µg/ml G418 (Gibco). Human dermal fibroblast primary cells, as well as MPS-I and -IIIb from patients, were cultivated in DMEM containing 10% FBS (De Pasquale et al., 2018b).

### Plasmids, cell transfections, and silencing

All purchased and supplied plasmids are listed in the [key resources table](#). 5xCLEAR-SV40-luciferase were got cloning 5xCLEAR elements upstream (KpnI-HindIII) the SV40 minimal promoter (Promega, pGL3 vector). Plasmid transfections were performed as previously reported (Ciano et al., 2016; D'Agostino et al., 2014; D'Agostino et al., 2019) by using X-tremeGENE HP DNA Transfection (Roche Italia, Monza MB, Italy), according to the manufacturer's protocol. Briefly, 3 µl of transfection reagent was mixed with 1 µg of DNA and incubated for 30 minutes at room temperature before being added to the cell cultures. Cells were grown for 24 hours of transfection before being collected for further experimental procedures. Silencing experiments were performed by using Lipofectamine 2000 transfection reagent (Thermo Fisher Scientific, US) and 100 nM of siRNA and 48 hours were used as setting conditions for each experiment.

### Immunoblotting

Total protein cell extracts were performed in a buffer (50 mM HEPES, 150 mM NaCl, 1 mM EDTA, 1 mM EGTA, 10% glycerol, and 1% Triton-X-100) supplemented with protease and phosphatase inhibitors (Cerullo et al., 2014). Protein concentration was estimated by a Bradford assay. Protein separation was made on SDS gels and transferred to PVDF membranes. Membranes were treated with a blocking solution (25 mM Tris, pH 7.4, 200 mM NaCl, 0.025% TWEEN20) containing 5% non-fat powdered milk and incubated overnight with primary antibodies. Membranes were incubated with an HRP-conjugated secondary antibody, and chemiluminescence was determined using the ECL detection system. Densitometric analysis was performed using the NIH Image software (Bethesda, MD, USA).

### Fluorescence microscopy

Immunofluorescence staining was performed as previously reported (Ciano et al., 2016; D'Agostino et al., 2014; D'Agostino et al., 2019). Briefly, cells were grown on glass coverslips, washed with PBS, and fixed in 3.7% formaldehyde at room temperature for 30 min or 100% methanol at -20 °C for 5 min. After fixation, cells were washed with PBS and permeabilized by incubation in blocking buffer (PBS containing 1% BSA, 0.01% sodium azide and 0.02% Saponin) for 10 min at room temperature. Cells were then incubated with the indicated primary antibodies diluted in the same blocking buffer for 1 h at room temperature. After three washes with PBS, cells were incubated with the corresponding secondary antibodies for 30 min at room temperature. Finally, coverslips were washed in distilled water and mounted onto glass slides with the Prolong Gold anti-fade reagent with DAPI (#P36935 Invitrogen, USA). Images were collected using confocal microscope LSM700 (Carl Zeiss Microimaging, Inc. Jena, Germany) equipped with a planapo 63× oil immersion (NA 1.4) objective lens. Z-slices were collected from the top to the bottom of the cells, and 3D reconstruction was carried out using LSM 700 software. Time-lapse analysis was performed as previously reported (D'Agostino et al., 2018). Pictures were taken with an UltraView Vox confocal spinning disk unit (PerkinElmer-Cetus, Waltham, MA) connected to an inverted Zeiss microscope (Carl Zeiss, Jena, Germany) equipped with a 100X oil immersion lens with a numerical aperture of 1.41 and two Hamamatsu Flash 4.0V2 cameras.

### Lysosome distribution and dispersion measurement

Lysosome distribution was quantified using Fiji software (Caiazza et al., 2019). Individual cell ROIs were outlined and whole cell Lamp1 signal fluorescence was measured. ROI was then decreased by 20% maintaining the same shape, and Lamp1 signal fluorescence was measured again. To generate a Lamp1 distribution curve, the signal intensity of each fraction was divided by the total cell signal. Twenty cells were quantified per cell treatment and averaged to quantify the population of lysosome distribution. Lysosome dispersion was measured by analyzing lysosomes distribution within the cells before and after incubation with the microtubule-depolymerizing agent Nocodazole at 10 µM for 2 hours to the cells exposed or not with LEU-ME 10 mM for 2 hours and fixed in methanol 100%.

### Ionomycin treatment and $\beta$ -hexosaminidase release assay

Confluent monolayers of cells in 60-mm culture dishes were washed with PBS and incubated with 500  $\mu$ l of ionomycin buffer (5  $\mu$ M ionomycin dissolved in PBS1X) for 5 minutes. The incubation buffer was collected and centrifuged at 11,000 g for 5 minutes before performing  $\beta$ -hexosaminidase release assay. Total cell extracts were obtained by incubating culture dishes with 500  $\mu$ l of lysis buffer (50 mM HEPES, 150 mM NaCl, 1 mM EDTA, 1 mM EGTA, 10% glycerol, and 1% Triton-X-100) supplemented with protease and phosphatase inhibitors. For each experimental point, 350  $\mu$ l of the ionomycin buffer was incubated for 20 minutes at 37°C with 50  $\mu$ l of 6 mM 4-methyl-umbellyferyl-*N*-acetyl- $\beta$ -D-glucosaminide in sodium citrate-phosphate buffer, pH 4.5. The reaction was stopped by adding 100  $\mu$ l of 2M Na<sub>2</sub>CO<sub>3</sub> and 1.1 M glycine, and the fluorescence was measured at excitation 365 nm/emission 450 nm. To determine the total cellular content of  $\beta$ -hexosaminidase, cell extracts were diluted 1:10 and 350  $\mu$ l was used for enzyme detection. The day before ionomycin treatment, cells were handled with U18666A 100  $\mu$ M or Chymostatin 100  $\mu$ M and incubated at 37°C for 24hrs.

### RNA isolation and real-time PCR

HeLa cells have been plated in a 6-multiwell. Once at 80% confluence, they have been treated with LEU-ME 10mM for 2h. Every well has been lysed in 1mL of TRIsure (BIOLINE, Cat No. BIO-38033) for 5 minutes. Total RNA has been extracted according to manufacturer protocol. 1ug of total RNA has been retrotranscribed with High-Capacity RNA-to-cDNA Kit (Applied Biosystems, REF 4387406), following manufacturer protocol. 2 ng of cDNA has been assayed for LC3A expression through real-time PCR, using SensiFAST SYBR Lo-ROX 2x Mix (Meridian, Cat No. BIO-94020) and the following primers at concentration 400nM:

LC3A: Fw: 5'-GTGAGTGTGCCACGCCCAT-3'

Rv: 5'-AGGTTTCCTGGGAGGCGTAG-3'

GAPDH: Fw: 5'-GTCGGAGTCAACGGATTGG-3'

Rv: 5'-AAAAGCAGCCCTGGTGACC-3'.

Real-time PCR has been performed in MicroAmp Fast Optical 96-Well Reaction Plate with Barcode 0.1mL (Applied Biosystems – REF 4346906), sealed with Optical Adhesive Covers (Applied Biosystems – REF 4360954). The reaction has been performed using QuantStudio 7 Flex instrument (Applied Biosystems) and software QuantStudio 6 and 7 Flex (Applied Biosystems). Expression level was calculated according to the  $2^{-\Delta\Delta CT}$  method (Livak and Schmittgen, 2001) by using *GAPDH* as a control gene. The data are presented as fold changes relative to the indicated reference sample.

### Luciferase reporter assays

HeLa cells were seeded in six multiwells and transfected with 0.5  $\mu$ g of the indicated luciferase reporter vectors plus 0.05  $\mu$ g of the renilla luciferase and cultured in a full medium for 24 h. Cells were then treated or not with the LEU-ME for 2 hours and finally lysed in reporter lysis buffer (Promega). Firefly and Renilla luciferase activities were measured in a luminometer using the Dual-Glo Luciferase assay kit (Promega). The relative luciferase activity (RLU) is defined as the firefly to-renilla luciferase activity ratio and normalized for the protein concentration of each sample. In all experiments, the values are reported as the average and standard deviations of three independent experiments carried out in triplicate. Statistical analysis was performed using Student's *t*-test.

### Quantification of the steric hindrance

The steric hindrance effect was quantified by measuring the number of cells displaying black areas (areas of the cells not populated by ER membranes) occupied by the enlarged lysosomes.

### QUANTIFICATION AND STATISTICAL ANALYSIS

All data are expressed as mean  $\pm$  S.D obtained by three independent experiments. Statistical analysis was performed by One-way ANOVA and Student's *t*-test. *p*-values are shown as asterisks: \*\*\* for  $p < 0.001$ , \*\* for  $p < 0.01$ , \* for  $p < 0.05$  and ns when data were not statistically significant.